Rare Metal Materials and Engineering
Volume 54, Issue 3, March 2025
Available online at www.rmme.ac.cn

Science Press

Cite this article as: Wang Bing, Li Chunyan, Wang Xinhua, et al. Progress on Microstructure and Performance Optimization in H/MEAs Regulated by Single and Hierarchical Heterostructures[J]. Rare Metal Materials and Engineering, 2025, 54(03): 640-664. DOI: https://doi.org/10.12442/j.issn.1002-185X.20240564.

REVIEW

Progress on Microstructure and Performance Optimization in H/MEAs Regulated by Single and Hierarchical Heterostructures

Wang Bing[1,2], Li Chunyan[1,2,3], Wang Xinhua[2], Li Xiaocheng[1,2], Kou Shengzhong[1,2,3]

[1] State Key Laboratory of Advanced Processing and Recycling of Nonferrous Metals, Lanzhou University of Technology, Lanzhou 730050, China; [2] School of Materials Science and Engineering, Lanzhou University of Technology, Lanzhou 730050, China; [3] Wenzhou Engineering Institute of Pump & Valve, Lanzhou University of Technology, Wenzhou 325105, China

Abstract: The development of high-performance structural and functional materials is vital in many industrial fields. High- and medium-entropy alloys (H/MEAs) with superior comprehensive properties owing to their specific microstructures are promising candidates for structural materials. More importantly, multitudinous efforts have been made to regulate the microstructures and the properties of H/MEAs to further expand their industrial applications. The various heterostructures have enormous potential for the development of H/MEAs with outstanding performance. Herein, multiple heterogeneous structures with single and hierarchical heterogeneities were discussed in detail. Moreover, preparation methods for compositional inhomogeneity, bimodal structures, dual-phase structures, lamella/layered structures, harmonic structures (core-shell), multiscale precipitates and heterostructures coupled with specific microstructures in H/MEAs were also systematically reviewed. The deformation mechanisms induced by the different heterostructures were thoroughly discussed to explore the relationship between the heterostructures and the optimized properties of H/MEAs. The contributions of the heterostructures and advanced microstructures to the H/MEAs were comprehensively elucidated to further improve the properties of the alloys. Finally, this review discussed the future challenges of high-performance H/MEAs for industrial applications and provides feasible methods for optimizing heterostructures to enhance the comprehensive properties of H/MEAs.

Key words: heterogeneous structures; H/MEAs; HDI effect; microstructure regulation; performance optimization

1 Introduction

The development of advanced metallic materials with optimal comprehensive performance to meet the growing demand in industrial fields is a pressing issue[1]. In recent years, high- and medium-entropy alloys (H/MEAs) have attracted increasing attention because of their extraordinary strength-ductility combination at room/cryogenic temperatures[2], superior corrosion resistance and wear resistance, excellent properties under extreme conditions, such as strong irradiation, superhigh temperature, hypervelocity impact[3–4], and considerable hydrogen storage capacity[5], which have demonstrated enormous potential for industrial application in the fields of aerospace, aircraft manufacturing and national defense equipment[6].

H/MEAs, also called the multi-principal element alloys (MPEAs) [1,7], are characterized by an extraordinary mixing entropy dominated by the addition of multiple elements in equal or nearly equal ratios (the concentration of each constituent element changes from 5at% to 35at%)[8]. In 2004, Yeh and Cantor proposed the MPEA concept. Subsequently, H/MEAs have been increasingly developed, and novel H/MEAs have been developed by combining various elements according to the design criteria for H/MEAs[9]. Based on the

Received date: August 29, 2024
Foundation item: National Natural Science Foundation of China (52261032, 51861021, 51661016); Science and Technology Plan of Gansu Province (21YF5GA074); Public Welfare Project of Zhejiang Natural Science Foundation (LGG22E010008); Wenzhou Basic Public Welfare Scientific Research Project (G2023020); Incubation Program of Excellent Doctoral Dissertation-Lanzhou University of Technology
Corresponding author: Li Chunyan, Ph. D., Professor, State Key Laboratory of Advanced Processing and Recycling of Nonferrous Metals, Lanzhou University of Technology, Lanzhou 730050, P. R. China, E-mail: lichunyan@lut.edu.com

addition of different elements, the intrinsic microstructural characteristics of H/MEAs can be divided into face-centered cubic (fcc), body-centered cubic (bcc) and hexagonal close-packed (hcp) systems. The notable H/MEAs contain 3D transition high-entropy alloys (THEAs), refractory high-entropy alloys (RHEAs), lightweight high-entropy alloys (LHEAs), lanthanide high-entropy alloys, noble metal high-entropy alloys, eutectic high-entropy alloys (EHEAs), high-entropy superalloys (HESAs) [10], such as AlCoCrFeNi, CoCrNi, FeCoCrNiMn, HfTaTiZr, CoCrFeNi, and CoNiV, and other H/MEAs composed of these alloys in combination. Moreover, fcc H/MEAs generally exhibit exceptional resistance to damage and high fracture toughness, and bcc H/MEAs exhibit high strength, hardness, friction and wear resistance[10]. However, there are also some bottlenecks in the overall performance of fcc and bcc H/MEAs.

It is widely known that the exceptional performance of H/MEAs mainly originates from their four unique core effects, which include high-entropy effect, sluggish diffusion effect, severe-lattice-distortion effect, and cocktail effect. However, some vital strengthening mechanisms exist to improve the overall performance of H/MEAs. It is widely accepted that the solution-strengthening effect of H/MEAs is remarkably higher than that of conventional alloys, owing to their multi-principal characteristics. Based on the size of the solute atoms, solution strengthening is mainly classified as substitutional or interstitial strengthening. In general, interstitial strengthening has a stronger strengthening effect than substitutional strengthening because the former generally induces tetragonal distortion in the lattice, producing a shear field that strongly interacts with the edge, screw, and mixed dislocations[6,8]. Grain-boundary (GB) strengthening is another important mechanism for H/MEAs performance optimization[8]. Because the Hall-Petch strengthening coefficient k is larger than that of the traditional alloy, H/MEAs show a stronger GB strengthening effect than the traditional alloy. The origin of GB strengthening in H/MEAs is the significant resistance to dislocation slip and misfit in the orientation between adjacent grains[6]. Precipitation strengthening can significantly optimize the mechanical properties of H/MEAs through endogenous advantageous strengthening phases (such as $L1_2$, B2, σ, Laves, and carbide precipitation) and exogenous particles[6,8]. It has been reported that the size, morphology, volume fraction, distribution of precipitates and interface relationship between the precipitates and the matrix are notable factors for the precipitation strengthening effect. Moreover, according to the size and interface relationship between the precipitates and matrix, precipitation strengthening is classified as shearable (small-sized precipitates and a coherent relationship) and Orowan bypass mechanisms (large size or an incoherent relationship)[8,11–12]. Dislocation slip is a common deformation mechanism observed in all metallic materials. For H/MEAs, the dislocation density increases with the increase in plastic strain, which can promote the interaction between dislocations from different slip planes and finally act as obstacles to the further motion of dislocations, leading to a strengthening effect[8,12]. In principle, there are also other strengthening mechanisms for enhancing the strength of H/MEAs, such as short-, medium-, and long-range ordered (SRO, MRO, LRO) strengthening.

However, the improvement of traditional H/MEAs is tightly related to the single-phase solid solution, local chemical SOR and increased lattice distortion[13], which exhibit some restrictions in upgrading performance of H/MEAs. For example, the fcc H/MEAs usually present inadequate yield strength (YS) and the bcc alloys show poor ductility and fracture toughness[6,9]. To overcome the property restrictions of H/MEAs, both the effective alloying and thermo-mechanical processing (TMP) routes are used to modify the microstructure, change deformation mechanisms and finally optimize the comprehensive properties of H/MEAs[13]. After rational alloying or moderate TMP, some new secondary phases and novel microstructures are introduced into H/MEAs, such as $L1_2$, B2, topologically close-packed (tcp) phases and more importantly heterogeneous structures[14]. Meanwhile, a large number of stacking faults (SFs), deformation twins (DTs), SF-based substructures and Lomer-Cottrell (L-C) locks are also discovered in H/MEAs, which effectively alter the deformation mechanisms of H/MEAs and eventually improve their properties[15].

Recently, architecting heterogeneous structures has been considered as one of the most available strategies to tremendously promote the performance of metallic materials[1]. It has been reported that the heterogeneous structures have been widely used to modify the overall performance of traditional alloys, such as Ti alloys, Ni-based superalloys, high manganese steels[16], Al alloys, Mg alloys, Cu alloys, Zn alloys and some composites and magnetic materials[17].

Inspired by the excellent comprehensive strength and toughness of natural biomaterials such as bamboo and shells, the concept of a heterogeneous structure has been proposed[18]. Wu et al[18] reported that the plastic deformation of heterostructures is a combined effect of geometrically necessary dislocations (GNDs) and forest dislocations. Heterogeneous units are critical in heterostructures. Currently, the widely studied heterogeneous units include grains, phases, defects (such as SFs, DTs with various sizes, morphologies, and dislocation cells), precipitates, and substructures[15]. These units can not only build heterostructures individually but also combine to form hierarchical heterostructures. The intrinsic characteristic of the optimized properties of heterostructure materials is the ultrahigh strain hardening induced by GNDs[19]. Hysteresis loops occur during the uniaxial and cyclic load-unload-reload (LUR) tensile testing of heterostructure materials, which mainly originate from the formation of back and forward stress caused by GND pileups[20]. The hysteresis loop emphasizes a more remarkable Bauschinger effect in the heterostructure sample and is also an iconic stress-strain response to heterogeneous deformation[20].

It has been proved that the deformation behavior of heterostructure samples presents heterogeneity (soft and hard domain), which results in the fact that the activation of

dislocations and stress state are different on both sides of the heterostructure interfaces[21]. At the initial deformation, the local stress at the heterostructure interfaces will firstly stimulate the dislocation source in the soft domain and subsequently trigger the dislocation pileup (deemed as GNDs) at the interface[21]. Furthermore, the increasing dislocation pileup will block the activation of the following dislocations. Therefore, supernumerary stress needs to be imposed to initiate more dislocations for the strain continuity[22]. The supernumerary stress on the one side of the heterostructure interfaces is called as back stress and there will be a corresponding stress according to the physical law on the other side, considered as forward stress. Both back stress and forward stress are collectively referred to as hetero-deformation-induced (HDI) stress[23].

There are many processes for preparing heterogeneous structures, such as alloying, heat treatment, and plastic deformation. Regarding alloying, it has been reported that the addition of elements C, N, O, B, and Si can be beneficial for the formation of compositional inhomogeneity in H/MEAs, such as short-range ordering (SRO) and medium-range ordering (MRO), which mainly originates from the difference in atomic radii and the sluggish diffusion effect[1,24–28]. Moreover, the heat-treatment processes, such as annealing, solid solution, aging, and homogenization, can promote the precipitation of different types of secondary phases, resulting in various stress states between the matrix and precipitates, thus inducing a strong HDI effect. More importantly, a combination of plastic deformation processes and heat treatment can be used to efficiently prepare heterogeneous structures in H/MEAs[10]. It has been proven that combining various rolling processes, powder metallurgy, pulsed laser processing, friction stir welding, selective laser melting, laser powder bed fusion, cold drawing, additive manufacturing (AM) processes, mechanical milling and spark plasma sintering processes, rotationally accelerated shot peening (RASP), surface mechanical attrition treatment (SMAT), facile laser surface remelting, ultrasonic nanocrystal surface modification (UNSM), hot forging, and high-pressure torsion (HPT) with reasonable heat-treatment processes can induce single and hierarchical heterostructures in H/MEAs. The deformation process and heat treatment can effectively modify the size and number of grains and phases in H/MEAs, and induce various defects (twins, interfaces, and SFs), which significantly contribute to the formation of heterogeneous structures in H/MEAs.

As mentioned above, the appearance of heterogeneous structures significantly improves the overall performance of traditional metallic materials owing to the distinctive strain hardening induced by HDI stress. In particular, heterogeneous structures are also promising for improving the comprehensive performance of H/MEAs[24]. Numerous studies have been conducted on the effects of heterostructures on the performance of H/MEAs, including their tensile properties at room or cryogenic temperatures, corrosion resistance, radiation resistance, and magnetic properties[25]. In this article, the relationship between the heterogeneous structure and overall performance of H/MEAs is systematically reviewed. The key points of this work include the heterostructure design for H/MEAs, the influence of heterostructure type on the performance of various H/MEAs, and further exploration of the intrinsic mechanisms of heterogeneous structures to optimize the alloy properties.

2 Heterogeneous Structures in HEAs

2.1 Regulation of single heterogeneity for HEA performance

Optimizing the properties of HEAs by constructing heterostructures has received increasing attention. Recently, multiple heterostructures have been discovered in HEAs, including compositional inhomogeneity, bimodal structures, dual-phase structures, lamella/layered structures, harmonic structures (core-shell), multiscale precipitates and heterostructures coupled with specific microstructures. Compared with hierarchical heterostructures, the single heterostructures solely ameliorate the performance and show some restrictions in modifying the microstructure of HEAs. This section will discuss the building method, microscopic characteristics, deformation mechanisms, and the effect of single heterostructures on the HEAs, performance and finally explore the effective strategies for optimizing the comprehensive performance of HEAs.

2.1.1 Compositional inhomogeneity

One of the most important core effects of HEAs is the high-entropy effect, which means that the element distribution in HEAs is highly disordered, and the lattice positions are randomly occupied by different atoms[26]. The high-entropy effect means that HEAs are inherently heterogeneous at the atomic scale[1]. The results of aberration-corrected transmission electron microscope (TEM) and high-angle annular dark-field scanning transmission electron microscope (HAADF-STEM) have proven that the atomic heterogeneity of HEAs and the distribution of elements in HEAs are highly random[27]. The random distribution of atoms with different radii can induce significant lattice strain, thereby enhancing the solid solution strengthening ability of HEAs and promoting their high intrinsic YS (high lattice friction)[27], particularly in bcc HEAs with significant atom size differences.

However, local chemical fluctuations (LCFs) exist in HEAs owing to the inhomogeneous distribution of elements induced by differences in atomic radii and binding forces[28]. For example, the occurrence of LCFs in the CoCrFeNiPd alloy can remarkably enhance both the strength and ductility of the alloy, compared with those of the CoCrFeNiMn alloy, which is attributed to the larger atomic radius and electronegativity of Pd[27,29]. It has been proven that LCFs can play a vital role in the inhibition of dislocation movement, thus significantly improving the work-hardening of HEAs[27]. Meanwhile, it is the addition of interstitial atoms that can improve performance of HEAs[26]. It has been reported that the addition of elements O, C, and N can boost the heterogeneity of HEAs due to the

formation of ordered structures, such as ordered oxygen complexes (OOCs)[30]. The ordered structures originating from the addition of interstitial atoms could retard the dislocation slips and interact with certain defects (SFs, DTs, and L-C locks), which not only affect the deformation mechanisms of HEAs but also enhance their strain-hardening ability, finally resulting in a balance between strength and ductility[26,31–32]. In the future, a promising strategy is to optimize the overall performance of HEAs by discovering more favorable interstitial atoms to induce more noticeable heterogeneity in them and regulate the size, distribution, and density of LCFs to further develop novel HEAs with excellent performance.

Moreover, the appearance of S/MRO is also beneficial for improving the comprehensive performance of HEAs[33]. The formation of S/MRO with the size of 1–2 nm is much easier when the binding enthalpies of elements are different[34–35]. As shown in Fig. 1, with the help of advanced characterization techniques, SRO with different sizes and volume fractions can be observed in VCoNi alloy[36]. In Fig. 1, CSRO refers to chemical SRO, and related selected-area electron diffraction (SAED) pattens can be ovserved. It has been reported that SRO can restrain dislocation movement due to higher lattice strain, which can increase the interaction between plenty of dislocations and accelerate dislocation tangles. Therefore, the formation of SRO is conducive to improving the work-hardening ability of HEAs and ultimately enhances the performance of HEAs[35]. Compared with SRO, MRO has larger size, which can more effectively hinder dislocation movement and improve HEAs' performance. Wang et al[37] discovered the heterogeneous MRO structure in $Al_{0.5}$CrCoNi HEAs. As mentioned above, MRO structure has larger size than SRO structure and thus can be hardly destroyed by dislocation slip, which will significantly optimize the properties of HEAs resulting from the stable MRO structure in HEAs[37]. In short, SMO and MRO structures are effective heterostructures for modifying microstructure and improving

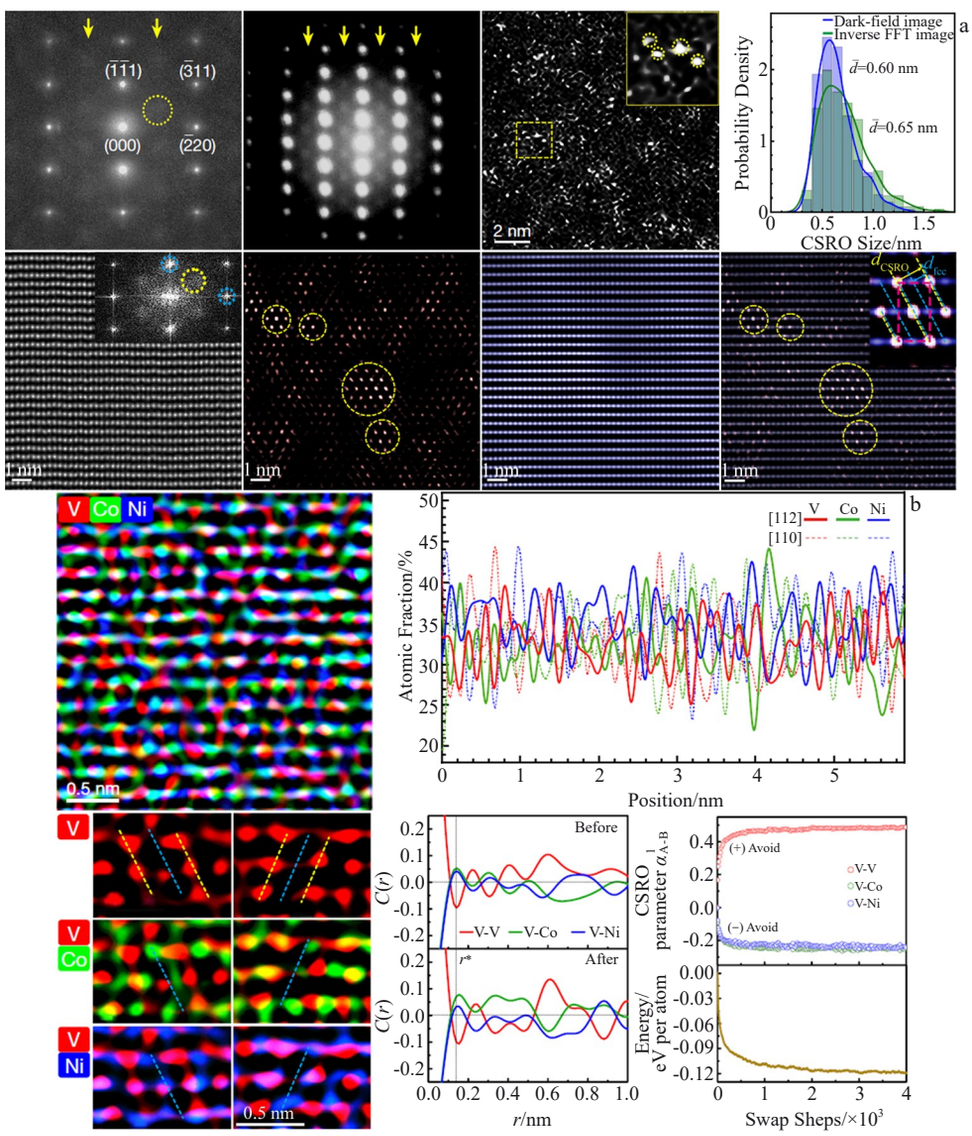

Fig.1 SRO in fcc VCoNi MEA[36]: (a) SAED patterns EDP with the [112] zone axis and nanobeam SAED pattern with the [112] zone axis; (b) chemical mapping indicating element-specific enrichment on alternating atomic planes

performance of HEAs. In addition, the contribution of S/MRO for the improvement of HEAs properties is restricted because of their nanoscale size, whereas the combination of S/MRO structure and other heterostructures can help to enrich the deformation mechanisms in HEAs and finally ameliorate the comprehensive performance of HEAs.

2.1.2 Bimodal structure

Bimodal structure is a highly important heterostructure in HEAs and mostly refers to a bimodal grain structure mainly composed of larger coarse grains and smaller recrystallized grains. The preparation methods for bimodal structures primarily include alloying (C, N-doped) and TMP such as rolling with various heat-treatment processes and powder metallurgy.

(1) Alloying and element-doping

Nanoscale TiC and TiO(C) particles were added to HEAs by mechanical alloying (MA) and spark plasma sintering (SPS) [38–40]. Chen et al[38] reported that the addition of TiC nanoparticles to the $Fe_{24}Ni_{24}Co_{24}Mn_{18}$ HEA was conducive to the preparation of the TiC/$Fe_{24}Ni_{24}Co_{24}Mn_{18}$ high-entropy composite (HEC). In HECs, TiC particles can stimulate the formation of heterostructures and optimize the YS with a relatively low coercivity of TiC/$Fe_{24}Ni_{24}Co_{24}Mn_{18}$ HEC. Meanwhile, introducing a non-uniform dispersion of TiO(C) nanoparticles in the CoCrFeNiMn HEA can effectively enhance the back stress and increase the resistance to forward stress in the heterostructure, resulting in an excellent strength-ductility synergy of the HEA[39]. Moreover, the nanosized TiC particles formed in situ can effectively regulate $Fe_{30}Ni_{30}Co_{29}$-$Cu_{5.5}Mn_{5.5}$ HEA microstructures, which is beneficial for the formation of a heterogeneous grain structure (HGS) in the alloy, thus optimizing the soft magnetic and mechanical properties of the HEA[40].

The trace element doped in HEA also shows a positive effect on the formation of bimodal grain heterostructure in HEAs. Zhang et al[31] pointed out that a unique heterogeneous bimodal grain was introduced in the CoCrFeMnNi HEA via N-doping. The N-doping will refine grains and simultaneously precipitate nanoscale Cr_2N particles, leading to the formation of heterostructure in the CoCrFeMnNi HEA. The addition of element C to CoCrFeNiMn HEAs could enhance the thermal stability of the microstructure. Meanwhile, C-doping promoted the $Cr_{23}C_6$ precipitation and thus suppressed the formation of brittle σ phases, which provoked the recrystallization process and was beneficial for the formation of fine grains via particle-stimulated nucleation mechanism, resulting in bimodal grain structures[41].

(2) Multiple rolling process

It is widely known that rolling with a subsequent heat-treatment process including annealing and aging is a practical process for forming heterogeneous bimodal grains in HEAs. In this review, the primary rolling processes include cold rolling, cryogenic rolling, hot/warm rolling, cyclic rolling, and combinations of multiple rolling processes. Fig. 2 shows the procedures of different rolling processes.

By a combination of cold-rolling and intermediate-temperature annealing, Wu et al[42] proposed a novel design strategy to develop a bimodal grain with characteristic dimensions ranging from the submicron to coarse-sized scale in the $Al_{0.1}$CoCrFeNi HEA, which resulted in a new generation of high-strength and high-ductility HEAs with a YS of 711 MPa, a UTS of 928 MPa, and a uniform elongation of 30.3%. A Co-free high-performance $Fe_{40}Mn_{10}Cr_{25}Ni_{25}$ HEA was developed by cold rolling, followed by annealing. The optimized mechanical properties of the alloy mainly originated from the deformation inhomogeneity caused by the bimodal grains composed of coarse non-fully recrystallized and fine recrystallized grains. Coarse grains were formed during the cold-rolling process, and a full recrystallization microstructure was induced with an increase in the annealing temperature[43]. Moreover, a bimodal structure composed of fully recrystallized grains of 25 μm in size surrounded by nano-sized grains was prepared by a simple cold rolling-annealing treatment process of the refractory $Al_2Nb_{53}Ta_{20}Ti_{15}$-$Hf_5$ alloy. In the alloy, the grain in soft region was strengthened via dislocation accumulation and dislocation interaction, and HDI strengthening was also introduced, which resulted in desirable mechanical properties of the $Al_2Nb_{53}Ta_{20}$-$Ti_{15}Hf_5$ alloy[44]. A prototypical fcc-based $Al_{0.3}$CoCrFeNi HEA exhibited a synergistic balance between strength and ductility owing to the HGS induced by cold rolling and subsequent annealing. The outstanding properties of the alloy are mainly attributed to strain partitioning and enhanced long-range back stress[45]. After two-step cold rolling and the corresponding annealing process, the CoCrFeNiMn fcc HEA overcame the

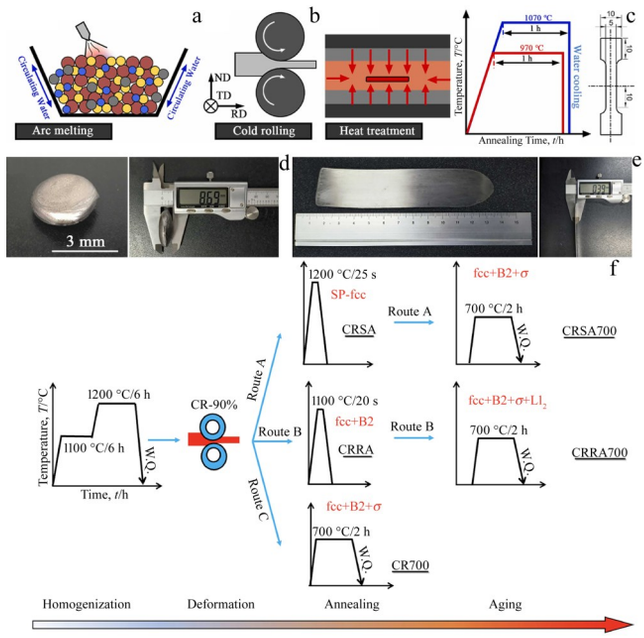

Fig.2 Schematic diagrams of various rolling process[13,44]: (a–c) cold rolling for $Al_2Nb_{53}Ta_{20}Ti_{15}Hf_5$ sample; (d) as-cast $Al_2Nb_{53}Ta_{20}$-$Ti_{15}Hf_5$ sample; (e) as-rolled $Al_2Nb_{53}Ta_{20}Ti_{15}Hf_5$ sample; (f) rolling with as-rolled different heat-treatments processes of $Al_{7.5}Co_{20.5}Fe_{24}Ni_{24}Cr_{24}$

restrictions of the strength-ductility trade-off owing to its HGS and reduced stacking fault energy (SFE), achieving a YS of 980 MPa, a UTS of 1385 MPa, and tensile elongation to failure (El.) of 48%. Multiple deformation mechanisms exist in the CoCrFeNiMn alloy, including HDI hardening, deformation twinning, Frank-Read dislocation sources, and L-C locks induced by such structures, which contribute to its excellent properties[46]. After simple cold rolling and annealing, a heterogeneous structure with $L1_2$ precipitates ranging from approximately 10 nm to 100 nm in size was observed in the $Ni_2CoCrFeTi_{0.24}Al_{0.2}$ HEA. Various deformation mechanisms, particularly HDI hardening, precipitation hardening and dislocation strengthening, were responsible for the superior mechanical properties, with a YS and El. of approximately 1.3 GPa and 20%, respectively[47]. Man et al[48] developed a complex $(Ni_2FeCoCr)_{88.25}Al_5Ti_3W_{1.5}Mo_{1.5}Nb_{0.75}$ HEA with a superior strength-ductility combination owing to the heterogeneous recrystallized and non-recrystallized matrix grains with abundant defects and secondary phases. Both the heterogeneous bimodal grains and advantageous microstructures were induced by a combination of cold rolling, annealing, and aging process. Similarly, a combination of simple cold rolling, annealing and aging significantly modified the microstructure of the $Co_{34.25}Cr_{15}Ni_{24}Fe_{15}$-$Al_5Ti_3W_{1.5}Mo_{1.5}Nb_{0.75}$ HEA. The process introduced a heterogeneous microstructure consisting of fine recrystallized grains and a deformed matrix, and simultaneously resulted in a large number of defects and precipitates in the heterogeneous microstructure, resulting in a YS of approximately 2.2 GPa and a promising El. of approximately 11.0%[49]. Furthermore, other HEAs, such as $(Fe_{57.5}Co_{20}Cr_{12.5}Ni_5Mo_3V_2)_{99.8}C_{0.2}$[50], FeMnCoCr[51], $Fe_{39.5}Mn_{40}$-$Co_{10}Cr_{10}C_{0.5}$[32] and $Al_{0.3}$CoCrFeNi[15], can also introduce the heterogeneous bimodal grain structure via cold rolling and subsequent heat-treatment processes to optimize the mechanical properties of the corresponding HEAs. More importantly, cold rolling followed by heat treatment can also induce numerous defects (dislocations, deformation twins, SFs and L-C locks), many secondary phases and even strain-induced martensitic transformation originating from metastability engineering, which is beneficial to the preparation of high-performance HEAs.

It is reported that cryogenic temperature rolling coupled with heat treatment is another effective method to induce heterogeneous bimodal grain structure in HEAs. Both $Al_{0.3}$CoCrFeNi[52] and $Al_{0.1}$CoCrFeNi HEAs[53] exhibit an ideal balance between strength and ductility owing to the heterostructure introduced by the cryogenic temperature rolling. HDI strengthening is the main method for improving the alloy performance. Meanwhile, after cryogenic temperature rolling, the specific transformation of fcc→9R phase→twin existed, resulting in the superior ductility and strain-hardening ability in $Al_{0.1}$CoCrFeNi HEAs because of twin-induced plasticity (TWIP) and phase transformation-induced plasticity (TRIP) effects[53]. By contrast, cryogenic temperature rolling and subsequent annealing also created HGS in single-phase fcc $FeCoCrNiMo_{0.2}$[10] and $CoCrFeNiMo_{0.2}$[54] HEAs. Furthermore, the optimized microstructures contained chemically ordered structures, an ordered $L1_2$ phase, and type 6^3 tcp phases in the $FeCoCrNiMo_{0.2}$ alloys, resulting in improved strain hardening owing to the outstanding performance of the alloy[10].

A combination of hot rolling and cold rolling is in favor of forming heterogeneous fine- and coarse-grained domains in a CrMnFeCoNi HEA[55]. Back-stress strengthening and multiple deformation mechanisms were responsible for the high strength and ductility of the alloy, which originated from the deformation gradient and the GND density[55]. Moreover, cyclic rolling and annealing were also helpful for the formation of HGS in $Al_{0.1}$CoCrFeNi HEA[56]. High HDI stress and various deformation mechanisms contributed to an ultra-high El. of approximately 53% and a UTS of 1165 MPa in $Al_{0.1}$CoCrFeNi HEA[56]. Fig. 3 shows a mixture of bimodal grain structures and optimized microstructures in HEAs, in which HDDs refer to high-density dislocations and KAM indicates kernel average micorientation.

(3) Powder metallurgy

Powder metallurgy is a facile strategy for forming HGSs to significantly enhance the overall performance of HEAs. Jiang et al[57] successfully prepared a CoCrFeMnNi HEA with a heterogeneous structure and a large range of grain sizes from 140 μm to 5 μm via high energy ball milling and SPS route, leading to a high YS over gigapascal level and a uniform elongation of 9.5%. After implementing MA and SPS, and introducing Y_2O_3 nanoparticles, a novel oxide dispersion-strengthened $Ni_{26}Co_{26}Fe_{25}Cu_{17}Ti_6$ HEA was developed, which displayed a significant bimodal grain microstructure in which abundant Y_2O_3 nanoparticles were distributed exclusively in the fine-grained region, thus modifying the size and fraction of the fine-grained region[58]. MA and SPS were also used to prepare a $Ni_2CoCrFeTi_{0.2}$ HEA with a HGS and dispersed oxide nanoparticles. The alloy exhibited a high YS of approximately 1070 MPa and an appreciably uniform El. of 11.6%, which was mainly attributed to the GB strengthening, oxide-dispersion strengthening, back stress strengthening/hardening and dislocation hardening[59]. Peng et al[60] developed a power hot extrusion method followed by annealing to design a dual-phase $AlCoCrFeNi_{2.1}$ eutectic HEA. After the power hot extrusion and corresponding heat treatment, a heterogeneous structure comprising both non-recrystallized and recrystallized grains with dense nanosized precipitates was observed in the alloy, leading to a superior YS of approximately 1.2 GPa, a UTS of approximately 1.5 GPa and a moderate El. of approximately 18%. The excellent tensile properties of the alloy primarily originated from the high strain hardening and accumulation of GNDs, which produced HDI hardening, grain refinement and nanoprecipitates[60].

Powder metallurgy is not only an effective strategy to form HGS, but significantly optimizes the microstructures of HEAs. After powder metallurgy, dispersing oxide nanoparticles and nanoprecipitates were introduced in HEAs, which can help form heterostructure and enhance properties of the HEA via remarkable precipitate strengthening. Accordingly, a

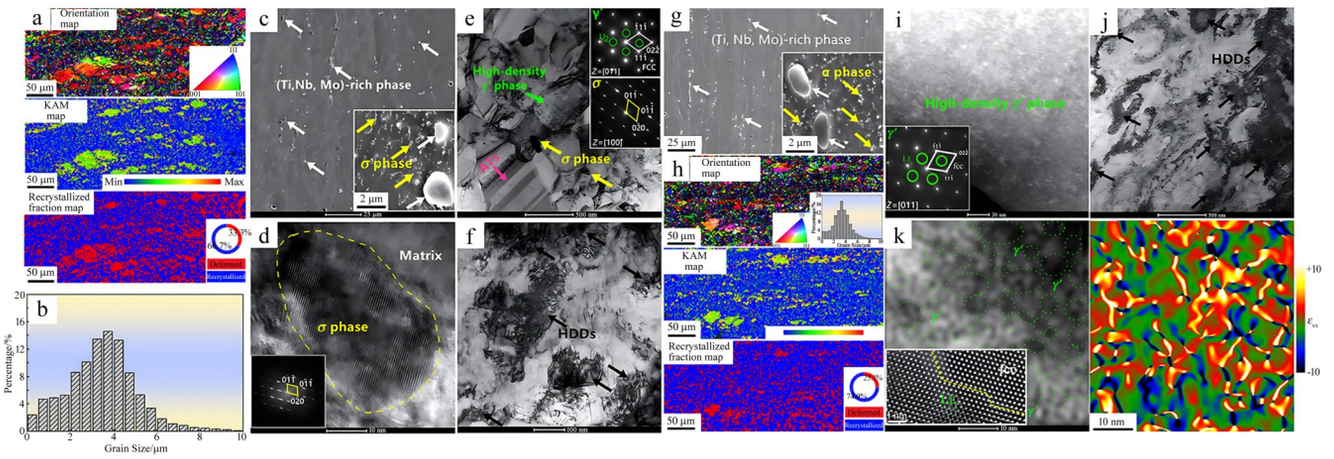

Fig.3 Mixture of bimodal grain structures and optimized microstructures in HEAs induced by rolling followed by heat treatments: (a, h) inverse pole figure (IPF) orientation map with the corresponding KAM map and recrystallized fraction map in different regions; (b) grain size distribution in recrystallized area of Fig.3a; (c, g) SEM images of (Ti, Nb, Mo)-rich phase and σ phase in different regions; (d) HRTEM image of σ phase with FFT pattern; (e) BF image of recrystallized region; (f, k) BF images of HDDs in deformed matrix; (i) HAADF image of high-density γ' precipitates; (j) HRTEM image with corresponding elastic strain map of γ' phases and elastic strain distribution[49]

combination of HGS with extrinsic nanoparticles and precipitates induced by powder metallurgy is a potential method for achieving the novel high-performance HEAs.

(4) Other techniques for forming bimodal grains

Shen et al[59] developed a spatially variable heterostructure of CoCrFeMnNi HEA using pulsed laser processing (Fig. 4). In Fig. 4, BM refers to base metal, FZ refers to fusion zone, and HAZ means heat-affected zone. There are two distinct preparation approaches: single-pass (SP) and double-pass (DP) laser passes. Compared to that prepared by the SP process, the alloy prepared by DP process displayed a sandwich-like structure with fine equiaxed recrystallized grains, which resulted in higher strength, ductility, and corrosion resistance because of the more uniform distribution of heterogeneity in the DP sample[59]. The $Al_{0.3}CoCrCu_{0.3}FeNi$ HEA was successfully prepared by friction stir welding (FSW) [61]. After the process, a fine-grained and partially recrystallized heterogeneous microstructure was observed in the alloy, which contributed to its superior tensile properties with a high YS of 920 MPa, high UTS of 1037 MPa, and good El. of 37%[61]. In addition, a heterogeneous eutectic microstructure consisting of columnar, equiaxed and L-shaped cells with much refined sizes down to nanoscales was constructed by selective laser melting (SLM) in the $AlCoCrFeNi_{2.1}$ eutectic HEA, leading to

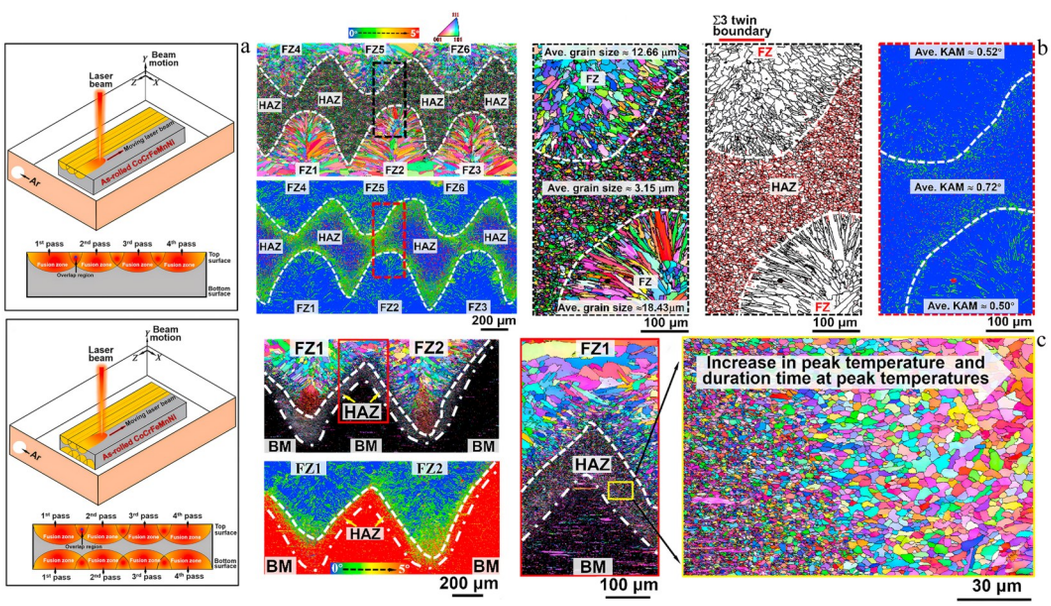

Fig.4 Schematic diagrams of preparation for spatially-variable heterostructure of CoCrFeMnNi HEA using pulsed laser processing (a); corresponding microstructures after pulsed laser processing (b–c) [59]

an ultrahigh YS of 982.1±35.2 MPa, a UTS of 1322.8±54.9 MPa, and an El. of 12.3±0.5%[62]. The improved properties mainly contributed to solid-solution strengthening, grain/cell-boundary strengthening and strain hardening from dislocations and nanoscale SFs[62]. SLM has also been used to optimize the high-cycle fatigue properties and deformation behavior of an equiatomic CoCrFeMnNi HEA[63]. The microstructure of the SLM-built alloy featured a HGS, dislocation network-induced substructures, and a high density of nanosized oxides, which are dispersed in the substructure and heterogeneous grain boundaries. The remarkable fatigue resistance of SLM-built alloys originates primarily from their HGS, dislocation networks and nano-sized oxides[63].

Kim et al[64] introduced a novel method for achieving the excellent combination of tensile strength and ductility in CrMnFeCoNi HEA at cryogenic temperature. The method consisted of laser powder bed fusion and the addition of interstitial atoms, which constructed a HGS and simultaneously the substructures as well as a high number density of nanosized oxides. A combination of heterostructure, substructures and nanosized oxides contributed to the superior mechanical properties and Charpy impact energies of the alloy at room/cryogenic temperature[64].

2.1.3 Dual-phase structure

(1) Advanced alloy design

To ameliorate the room-temperature brittleness of RHEAs, Han et al[65] prepared a novel TaMoZrTiAl RHEA via Zr doping. The microstructure of the alloy was significantly modified by the addition of element Zr. More importantly, the alloy showed a noticeable strength-plasticity synergy with high plasticity exceeding 20% and a high strength exceeding 2380 MPa, which was attributed to the specific dual-phase structure consisting of a hard disordered bcc phase embedded in a soft intermetallic B2 matrix[65]. The intrinsically improved performance of the alloy was due to solid solution strengthening, HDI strengthening, deformation-induced strain partitioning and dislocation cross-slip[65]. A novel heterogeneous $AlCoCr_2FeNi_2$ HEA was developed with dual-phase features of alternating fcc and bcc phases, which are mbedded in some B2 phases[66]. The addition of elements W and Co was also beneficial for forming heterogeneous dual-phase in $Co_{30}Cr_{30}(FeNi)_{40-x}W_x$[67] and CoCrFeNi[68] HEAs, respectively. Typical dual-phase structures are shown in Fig.5.

(2) Multiple rolling process

Xiong et al[69] developed a eutectic $AlCoCrFeNi_{2.1}$ HEA with an outstanding combination of high strength and excellent ductility using cold rolling followed by annealing and aging. After the TMP process, a dual-phase structure consisting of the fcc and B2 phases was prepared, and extensive nanoprecipitates were discovered in the dual-phases. The performance improvement mainly relied on dual-phase heterogeneous structure strengthening/hardening and obvious nanoprecipitate strengthening[69]. By firstly using cold rolling, then hot rolling, followed by annealing, a dual-phase (fcc and bcc) $Al_{18}Cr_{10}Fe_{10}Co_{27}Ni_{35}$ HEA was prepared, which showed a high YS of 1580 MPa, UTS of 1854 MPa, and good ductility of approximately

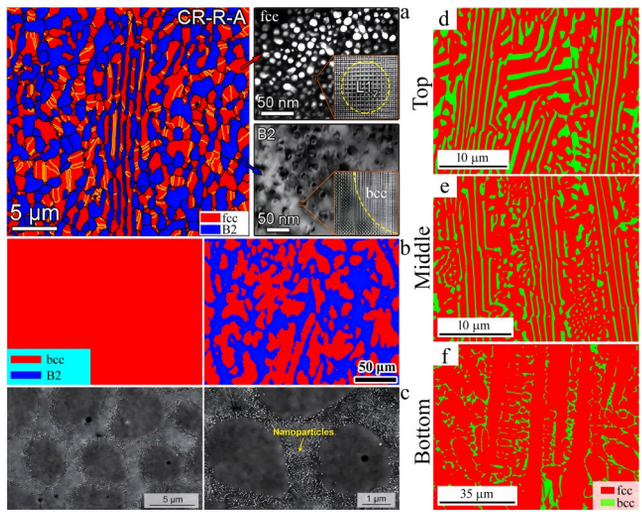

Fig.5 Various dual-phase structures in HEAs: (a) fcc and B2 phases in $AlCoCrFeNi_{2.1}$ EHEA[69]; (b) fcc and bcc phases in $AlCoCrFeNi_{2.1}$ EHEA[14]; (c) bcc and B2 phases in $(TaMoTi)_{92}Al_8$ RHEA[65]; (d – f) cellular-structured microstructure and high-density nanoparticles in $Co_{47}Ni_{28}Cr_{16}Fe_3Al_3Ti_3$ HEA[74]

18.4%[70]. Superior HDI hardening was achieved in the alloy owing to different flow stress areas. Good ductility primarily contributed to dislocation distribution, micro-strain band, and interaction between precipitates and dislocations[70]. The effect of annealing time on the microstructure and performance of a $FeCoNiAl_{0.25}Mn_{0.25}$ HEA sample was systematically studied[71]. A superior combination of mechanical and magnetic properties was discovered after annealing at 850 °C. And the microstructure comprised bcc precipitates, recrystallized fcc equiaxed grains and a few fcc hard-deformed lamellae[71]. Fig. 6 shows the interfacial structures and orientation relationships of the dual phases. The newly designed Co-free $Fe_{35}Mn_{15}Cr_{15}Ni_{25}Al_{10}$ HEA was rolled at room temperature and subsequently annealed and aged[72] (Fig.7–Fig.8). A dual-phase structure consisting of fcc and bcc or ordered B2 phases, was introduced into the alloy. However, many multiscale precipitates, including bulk primary B2-NiAl and secondary bcc/B2 particles with a wide size range, were also found in the alloy. Both the dual-phase structure and abundant precipitates significantly contributed to the overall performance of the alloy at room and cryogenic temperature[72].

(3) Other techniques for forming dual-phase structure

Inspired by bionic structures, after multipass cold drawing followed by annealing treatment, Zhou et al[73] developed an $AlCoCrFeNi_{2.1}$ EHEA with a bionic bamboo fiber heterogeneous dual-phase structure consisting of a hard-B2 fiber and soft fcc matrix. The alloy exhibited excellent synergy of strength and ductility owing to the remarkable HDI hardening caused by the deformation incompatibility and strain gradient between the dual phases[73].

Recently, AM processes have been shown to effectively produce dual-phase structures in HEAs.

Xiao et al[74] exploited the ability of AM to enable structural

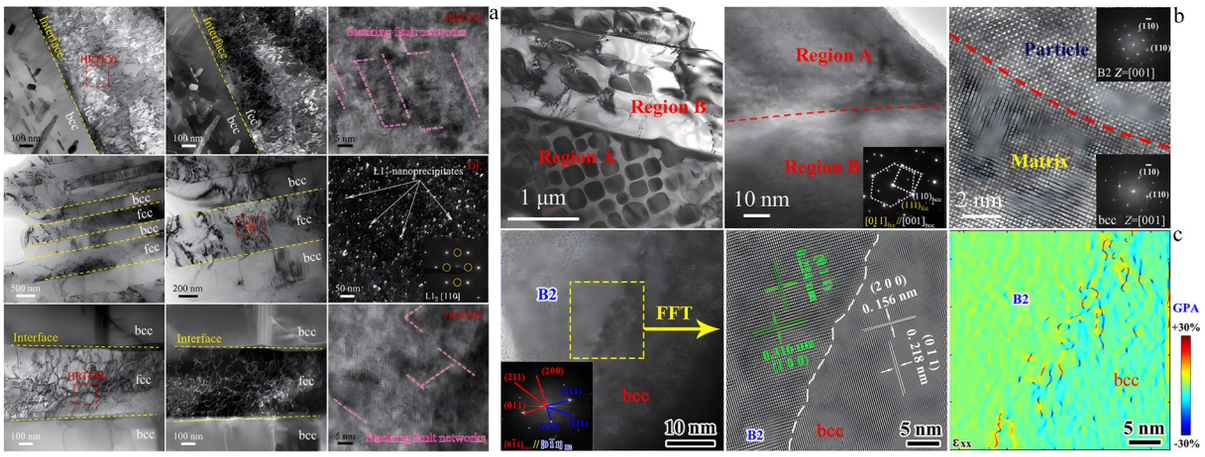

Fig.6 Interface structures and orientation relationship of dual-phases: (a) microstructure and dislocation substructure of HEAs[70]; (b) TEM analysis of $AlCoCr_2FeNi_2$ HEA[66]; (c) HRTEM image, FFT image, and GPA map of TaMoZrTiAl RHEA[65]

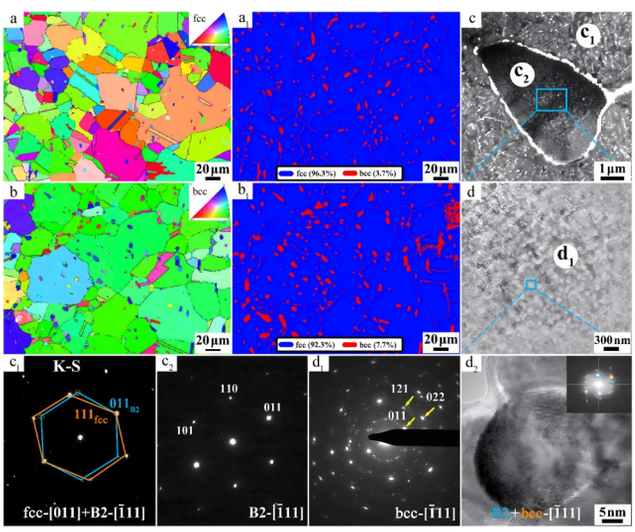

Fig.7 Orientation of dual-phases[72]: (a–b) IPF maps and (a_1–b_1) phase maps by A00 (a, a_1) and A10 (b, b_1) HEAs; (c) BF TEM image of A10 HEA; (c_1–c_2) corresponding SAED patterns of matrix and bulk B2-NiAl phase marked in Fig. 7c; (d) enlarged TEM image of nanoparticles in Fig. 7c; (d_1) SAED pattern of nanoparticles marked in Fig.7d; (d_2) HRTEM image

and compositional multiscale heterogeneity in HEAs and prepared a cellular-structured $Co_{47}Ni_{28}Cr_{16}Fe_3Al_3Ti_3$ HEA using directed energy deposition (DED) technique. After deposition, the alloy was featured with a prominent single-phase (fcc) interior and a dual-phase (fcc+$L1_2$) wall, resulting in an ultrahigh UTS of approximately 1148 MPa and high ductility of approximately 28%. The high-density $L1_2$ phases in the wall were responsible for the ultrahigh strength owing to order strengthening, and the high ductility mainly originated from excellent HDI hardening and high-density SFs[74]. A dual-phase $AlCoCrFeNi_{2.1}$ EHEA consisting of fcc ($L1_2$) and bcc (B2) phases was also prepared using the DED process[14]. Notably, the dual-phase structure was transformed into a lamellar structure composed of soft $L1_2$ and hard B2 phases with the prologation in DED time[14]. Dual-phases can provide considerable HDI hardening and restrain dislocation slip, thereby significantly optimizing the overall performance of the alloy[14]. Moreover, a heterogeneous fcc and bcc/B2 structure was introduced into the $AlCoCrFeNi_{2.1}$ EHEA using SLM, resulting in outstanding compressive properties of the alloy[75].

2.1.4 Lamellar or layered structures

The lamellar or layered structure is another desired hetero-structure for the enhancement of HEA performance. Zhang et al[76] prepared an aged Fe-27.5Ni-17.5Co-10.5Al-2.2Ta-0.04B HEA featuring a heterogeneous lamellar structure, which achieved high strength (over gigapascals) and a high El. of approximately 30%. Some lamellar microstructures are shown in Fig.9. Some complementary strengthening mechanisms consisting of a solid solution, interfaces, precipitation, and martensitic transformation are responsible for the high strength. Moreover, hetero-deformation modified by micro-bands and martensite phases contributes to reasonable ductility[76]. However, the unique elongated lamellar microstructure also improves the overall performance of the $AlCoCrFeNi_{2.1}$ EHEA. The lamellar structures provide substantial phase boundaries, resulting in boundary strengthening, and the lamellar fcc phases stimulate abundant cross-slip to enhance strain hardening. Furthermore, the lamellar bcc phases contribute to high strength because of significant precipitation hardening[77].

Rolling is a desirable strategy for forming lamellar structures, including cold rolling, warm rolling and a combination of cold and hot rolling.

Ma et al[78] prepared a high-performance $Zr_{35}Ti_{30}Nb_{20}Al_{10}V_5$ RHEA with a high YS of 1.1 GPa and a moderate El. of 20%. After rolling and subsequent annealing processes, the microstructures of the alloys were significantly modified, featuring a heterogeneous lamellar structure accompanied by high-density dislocation cells, dislocation pileups and lattice distortion in the local chemically ordered structure. The remarkable heterogeneous lamellar structure significantly contributed to the outstanding mechanical properties via HDI

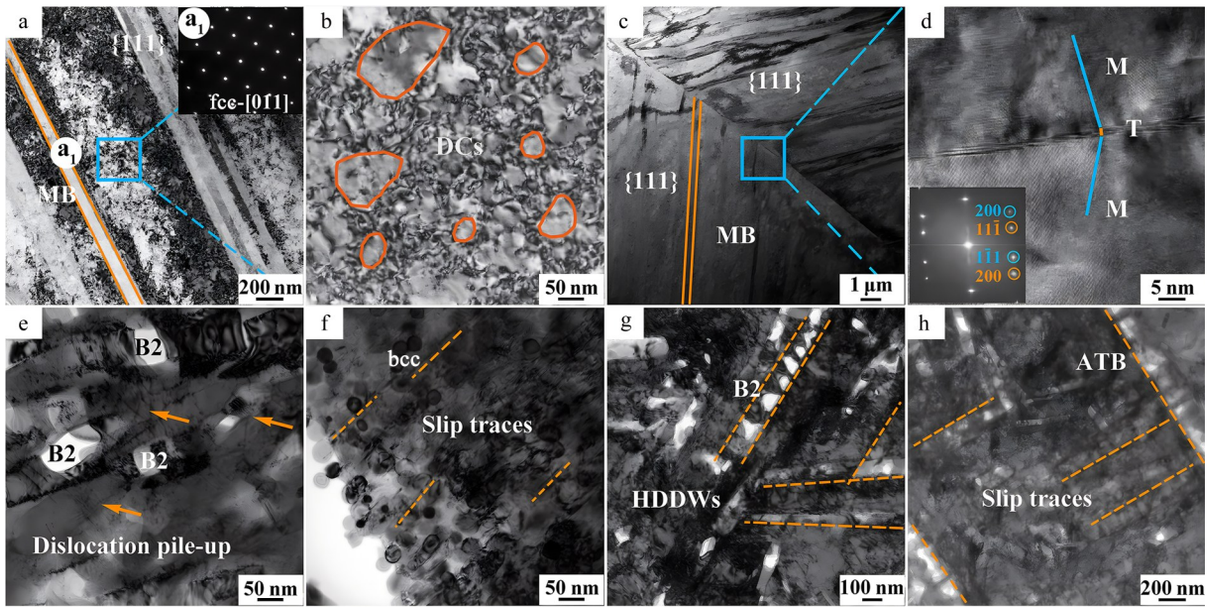

Fig.8 Defects in dual-phase structures of A00 (a–d) and A10 (e–h) alloys after tensile deformation: (a–c) BF TEM images for A00 HEA at 77 K; (d) HRTEM image and SAED pattern of twins in Fig.8c; (e–f) TEM images for A10 HEA at 293 K; (g–h) TEM images for A10 HEA at 77 K[72] (DCs mean dislocation cell structures; MB refers to microbands; HDDWs mean high-density dislocation walls, and ATB means annealing twin boundary)

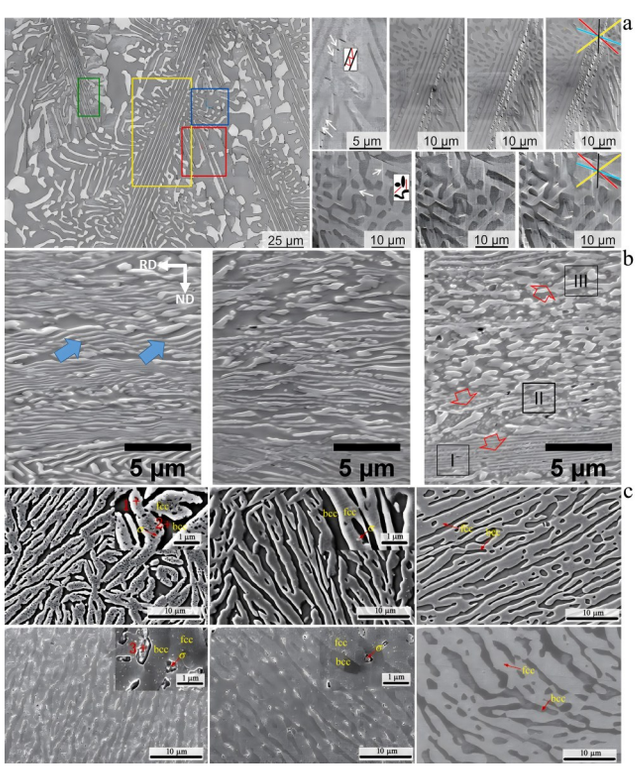

Fig.9 fcc and bcc lamellar microstructure in as-cast AlCoCrFeNi$_{2.1}$ EHEA (a) [77]; lamellar phases in $Al_{0.5}CoFeCrNiSi_{0.25}$ HEA (b) [79]; nanolamellar microstructure in AlCoCrFeNi$_{2.1}$ EHEA (c)[82]

hardening, and the microband-induced plasticity effect was beneficial for high ductility[78]. Meanwhile, cold rolling and annealing processes play a vital role in the formation of a lamellar structure containing fcc, bcc, σ, $L1_2$ and B2 phases, leading to a good combination of tensile strength (approximately 1267.8 MPa) and ductility (uniform El. of approximately 34.4%) in $Al_{0.5}CoFeCrNiSi_{0.25}$ dual-phase HEA[79]. It has been proven that these excellent properties are largely due to HDI straining and the fraction of fcc phases[79].

To significantly reduce or completely eliminate microstructural damage caused by the cold rolling process, Zhou et al[80] developed a novel warm rolling method to regulate the microstructure and improve the properties of $Zr_{45}Ti_{15}Nb_{30}Ta_{10}$ refractory complex concentrated alloys. A layered heterogeneous structure and considerable precipitates were induced by warm rolling, and an optimal strength-ductility combination was achieved in the alloys owing to the layered heterogeneous structure, subgrain boundaries and textures[80]. A continuous nanoscale lamellar structure composed of fcc and bcc (B2) phases was constructed in a cobalt-free $AlCrFe_2Ni_2$ HEA using a combination of warm rolling and annealing processes[81]. The annealing time has an important effect on the formation of the lamellar structure, which significantly optimizes the strength and ductility of the alloy[81]. Reddy et al[82] also conducted severe warm rolling and subsequent annealing to create a lamellar arrangement of ordered $L1_2$ and B2 phases in an AlCoCrFeNi$_{2.1}$ EHEA. After the deformation process, a mixture of lamellar and nonlamellar regions was deemed as a novel heterogeneous microstructure, which was helpful for the exceptional strength-ductility combination[82].

In addition, the combination of hot and cold rolling is a promising method for preparing lamellar and layered heterogeneous structures to regulate the performance of HEAs[83–85].

Using hot rolling followed by cold rolling, advantageous heterogeneous lamellar (HL) structures were successfully prepared in non-equiatomic FeNiCoAlCrB (NCACB)[84] and FeNiCoAlTaB (NCATB)[85] HEAs. In the NCACB alloy, the formation of the HL structure originated from the Zener pinning (NiAl, B2) effect and grain growth within large deformation bands, resulting in a remarkable HDI effect for performance improvement[84]. However, the mechanical properties of the NCATB alloy were different because of the variation in annealing time, which was regulated by multiscale HL structures. Similar to the NCACB alloy, the formation of the HL structure in NCATB was attributed to the Zener pinning effect of the NiAl (B2) phases[84]. In contrast to the previous two alloys, the formation of HL structures in a dual-phase $Al_{16}Cr_{20}Fe_{10}Co_{30}Ni_{24}$ HEA was related to cold rolling followed by hot rolling[83]. The HL structures were characterized by a combination of fcc and bcc (B2) phases, which significantly optimized the microstructures in the $Al_{16}Cr_{20}Fe_{10}Co_{30}Ni_{24}$ HEA, such as promoting recrystallization, precipitation and formation of numerous SFs[83]. The dual-phase HEA with the HL structure exhibited outstanding tensile properties, with a YS of 1120 MPa, UTS of 1540 MPa and El. of approximately 25% due to the noticeable heterostructures and optimized microstructures[83].

2.1.5 Harmonic structure (HS)

HS is a typical heterogeneous structure for the improvement of HEA performance. The remarkable characteristic of HS is that their microstructures are composed of a core and a shell (a periodic three dimensional network)[86]. During the deformation process, the stress/strain responding of the core and shell is different, which will induce noticeable HDI deformation features and ultimately regulate overall performance of HEAs. Fig.10 shows some HSs in different HEAs.

Zhang et al[87–88] prepared a HS CoCrFeMnNi HEA consisting of coarse-grained cores and ultrafine-grained shells. After mechanical milling and SPS process, different shell fractions existed in some alloys and the effect of shell fraction on the low-cycle fatigue (LCF) performances was studied in detail. The results showed that a combination of superior strength-ductility synergy and good LCF resistance was achieved when the shell fractions ranged from 20% to 40%[87]. Moreover, the effect of HS on the corrosion resistance of CoCrFeMnNi HEA was discussed[86]. Compared with the homogeneous grain structure (coarse grain or fine grain), the corrosion resistance mediated by the peculiar core-shell network structure was superior[86]. The HS is also beneficial for the fatigue crack growth (FCG) behavior in CoCrFeMnNi HEA[89]. The network core-shell structure can effectively strengthen roughness-induced crack closure by regulating crack deflection, resulting in a balance between mechanical properties and FCG resistance[89].

2.2 Regulation of hierarchical heterogeneity for HEA performance

Recently, hierarchical heterostructures have received widespread attention due to their more remarkable HDI effect, which contains gradient microstructure, bimodal grain coupled with some specific defects or phases, hierarchical heterogeneous phases, etc. In this section, the effect of hierarchical heterostructures on the regulation of microstructure and optimization of comprehensive properties for HEAs is discussed in detail and the optimal hierarchical heterostructures for optimizing HEA properties are further explored.

2.2.1 Gradient structure

RASP was used to create a hierarchical grain size gradient microstructure with a high nanotwin population in a

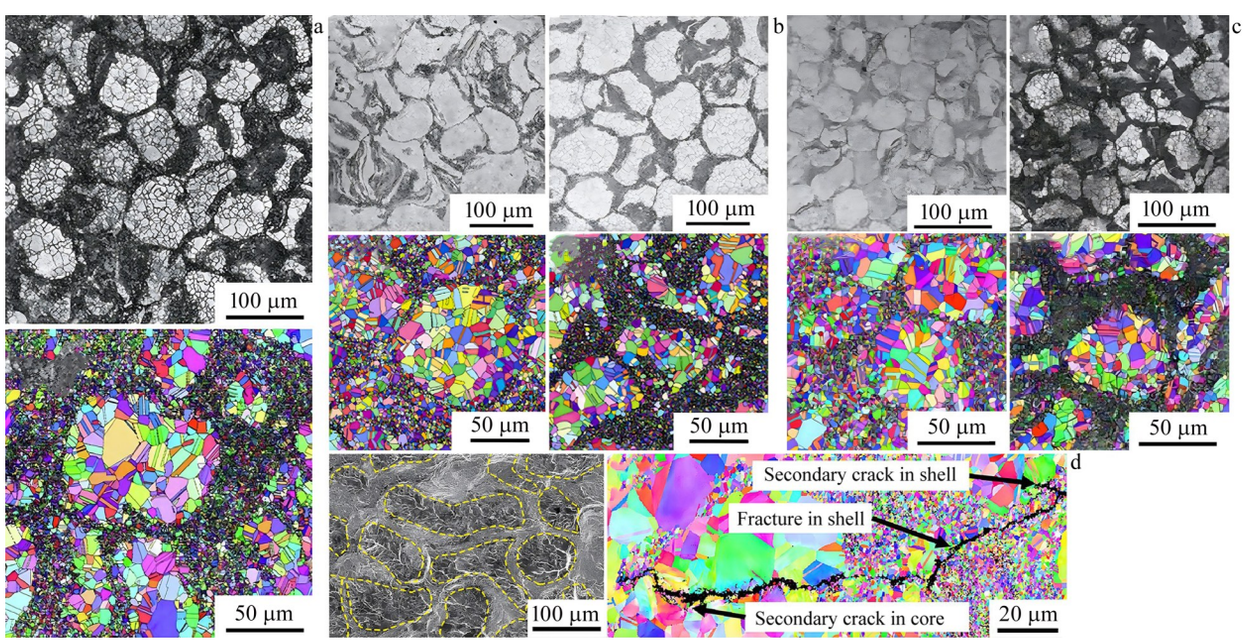

Fig.10 HS in different HEAs: (a – c) microstructures of the sintered CoCrFeMnNi HEAs[86–88]; (d) crack-path and fractography of sintered CoCrFeMnNi HEAs[89]

CoCrFeMnNi HEA[90]. Multiple strengthening and deformation mechanisms are responsible for the excellent mechanical properties of these alloys[90]. A novel gradient cell structure was created in a stable single-phase $Al_{0.1}$CoCrFeNi HEA[7]. Meanwhile, tiny high-density SFs and twins were generated by the gradient cell structure. Both the gradient cell structure and high-density defects contributed to the optimized properties of single-phase HEAs[7]. To avoid early strain localization at the nanostructured topmost layer, a novel gradient structure composed of gradient distributions for both the grain size and volume fraction of precipitates was designed in the $Al_{0.5}Cr_{0.9}FeNi_{2.5}V_{0.2}$ HEA using SMAT and an aging process[2]. The dual-gradient structures exhibited a stronger HDI effect because of severe strain gradients and higher GND density. Meanwhile, a high volume fraction of the B2 and $L1_2$ phases with a gradient distribution provided strong precipitation hardening[2]. A gradient nanostructured layer with a thickness of approximately 100 μm was prepared in a TiZrHfTaNb RHEA using a facile laser surface remelting-based surface treatment technique[91]. The grain size of the gradient nanostructured layer ranged from approximately 200 μm to only 8 nm in the top surface layer. More importantly, the wear resistance of the alloy was significantly enhanced by the formation of multiphase and gradient nanostructures[91].

Chen et al[92] developed high-strength and high-ductility $AlCoCrFeNi_{2.1}$ EHEA metallic wires at room and cryogenic temperature using multiple-stage heavy-drawn and heat-treated processes. A specific gradient structure composed of hard gradient-distributed B2 lamellae embedded in a soft fcc lamellar matrix was constructed in the alloy during deformation, which resulted in a radial gradient distribution of GNDs during tension and led to a high UTS of 1.85 GPa and El. of approximately 12% at room temperature as well as an ultrahigh UTS of 2.52 GPa and an El. of approximately 14% at cryogenic temperature[92]. Moreover, a combination of the heterogeneous gradient structure and optimized microstructures, including DTs, dense dislocations, SFs, L-C locks, phase transformation and the 9R phase, contributed to the superior performance of CoCrFeNi HEA microfibers[93]. Furthermore, both the mechanical properties and corrosion resistance of the CrMnFeCoNi HEA prepared by UNSM were simultaneously improved owing to the formation of a gradient structure with grain size variation from the surface to the center[94]. Multiple strengthening mechanisms have been introduced to achieve excellent mechanical properties and low surface roughness. The results showed that a small grain size and large compressive residual stress were responsible for the desired corrosion resistance[94]. The optimized gradient structures are shown in Fig.11.

2.2.2 Hierarchical heterogeneity composed of grains and phases

The $(CoCrFeNi)_{94}Ti_2Al_4$ HEA exhibited a superior combination of strength and ductility after liquid-nitrogen rolling, followed by partial recrystallization and aging heat treatments, which contributed to the formation of a multiscale heterogeneous microstructure comprising heterogeneous grain sizes, precipitates and grain defects[95]. The hierarchical heterostructures were highly beneficial for a high YS of 1 GPa, UTS of 1.2 GPa and good ductility of approximately 21% of the alloy originating from HDI strengthening and hardening[95]. Dasari et al[96] constructed a hierarchical heterostructure consisting of fcc grains with two different size distributions and B2 precipitates with two different size scales

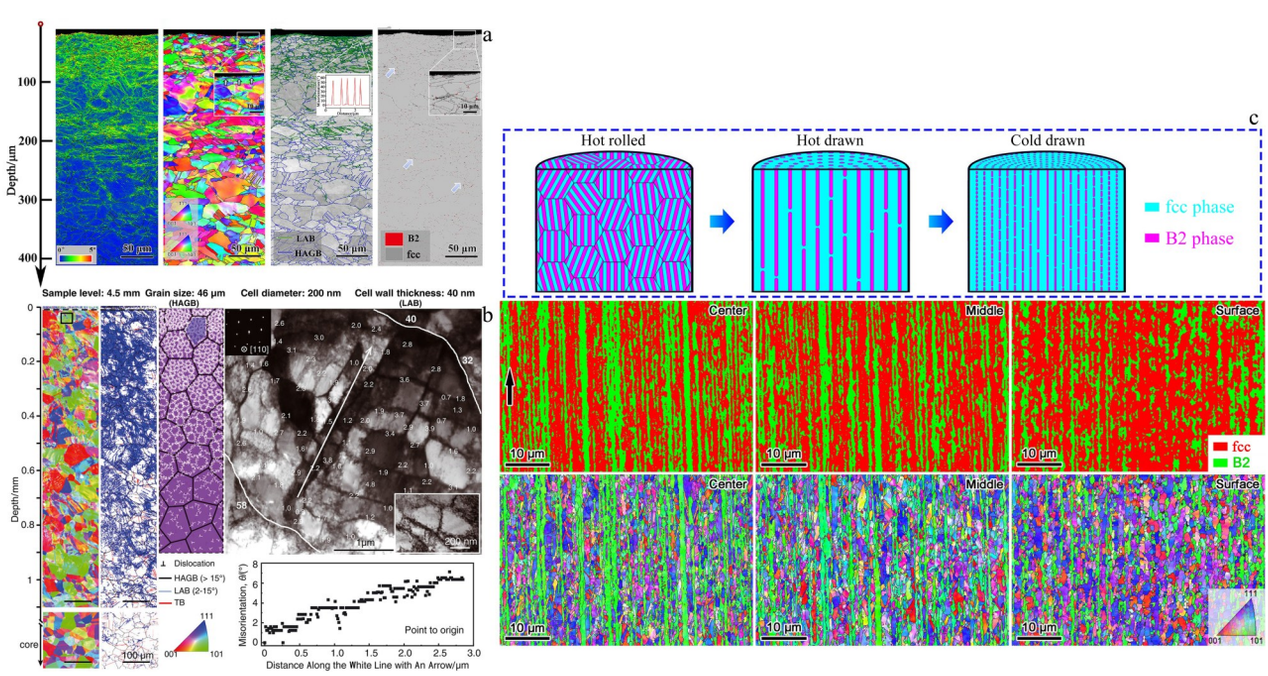

Fig.11 Typical gradient microstructure for the as-SMATed $Al_{0.5}Cr_{0.9}FeNi_{2.5}V_{0.2}$ HEA (a)[2]; structural gradient of a gradient dislocation structure (b)[7]; gradient heterogeneous lamella structure (c)[92]

in fcc $Al_{0.5}Co_{1.5}CrFeNi_{1.5}$ HEA via a brief TMP process. The optimized heterostructure significantly enhanced the YS and ductility of the alloy[96]. Zhao et al[97] explored the influence of various TMP processes on heterostructure formation (Fig. 12). The results showed that cold/cryogenic rolling processes at reasonably intermediate temperature were better for heterostructure formation than annealing at low temperature for a long time. The hierarchical structures are characterized by stretched original grains, surviving original grains, fully recrystallized equiaxed grains, and B2 precipitates induced by cold/cryogenic rolling followed by annealing at intermediate temperature[97]. The complex heterogeneous microstructure resulted in excellent properties of the $Al_{0.3}CoCrFeNi$ HEA, with a high UTS of approximately 1019 MPa and an El. of approximately 28%[97]. A $Nb_{55}Ta_{25}Ti_{15}Hf_5$ HEA with a combination of fine-grained, coarse-grained and HL structures was prepared by cold rolling, and balanced tensile properties[98] were obtained.

The addition of element C to the WTaMoNb RHEA supports the forming of hierarchical heterostructure via a spherical spray-granulated powder[99]. The dual-heterogeneous structure contained the fcc skeleton structure in the bcc matrix with dispersive fcc hard particles, which can markedly enhance the resistance to cracking, provide high formation quality and increase the hardness, fracture toughness, and elastic properties of the WTaMoNb RHEA[99]. A novel powder metallurgy-based severe plastic deformation (P-SPD) was used to tailor the heterostructure of an $AlCoCrFeNi_{2.1}$ EHEA[100]. Hierarchical heterogeneity was synthesized using powder metallurgy coupled with HPT, and consisted of nanoscale heterogeneity, including fcc and B2 phases, and microscale heterogeneity with hard and soft domains formed by a mixture of powder types[100]. Intense HDI strengthening was introduced by a hierarchical structure to achieve an enhanced YS of approximately 1.5 GPa in the alloy[100]. To release the potential of the recrystallization fraction for property consistency, heterogeneous precipitates were introduced into the heterogeneous grains of partially recrystallized $Ni_2CoCrFeTi_{0.24}Al_{0.2}$[101], as shown in Fig. 12. The formation of heterogeneous precipitates was attributed to discontinuous coarsening, which could effectively offset the reduced HDI stress caused by the increase in the dynamic recrystallization (DRX) fraction and improve the ductility. However, the desired strength of an alloy is regulated by both lamellar precipitates and GB strengthening[101].

By employing hot-forging and annealing, the dual-level heterostructures were formed in a carbon-doped fcc CuFeMnNi HEA[102]. The heterostructures were composed of

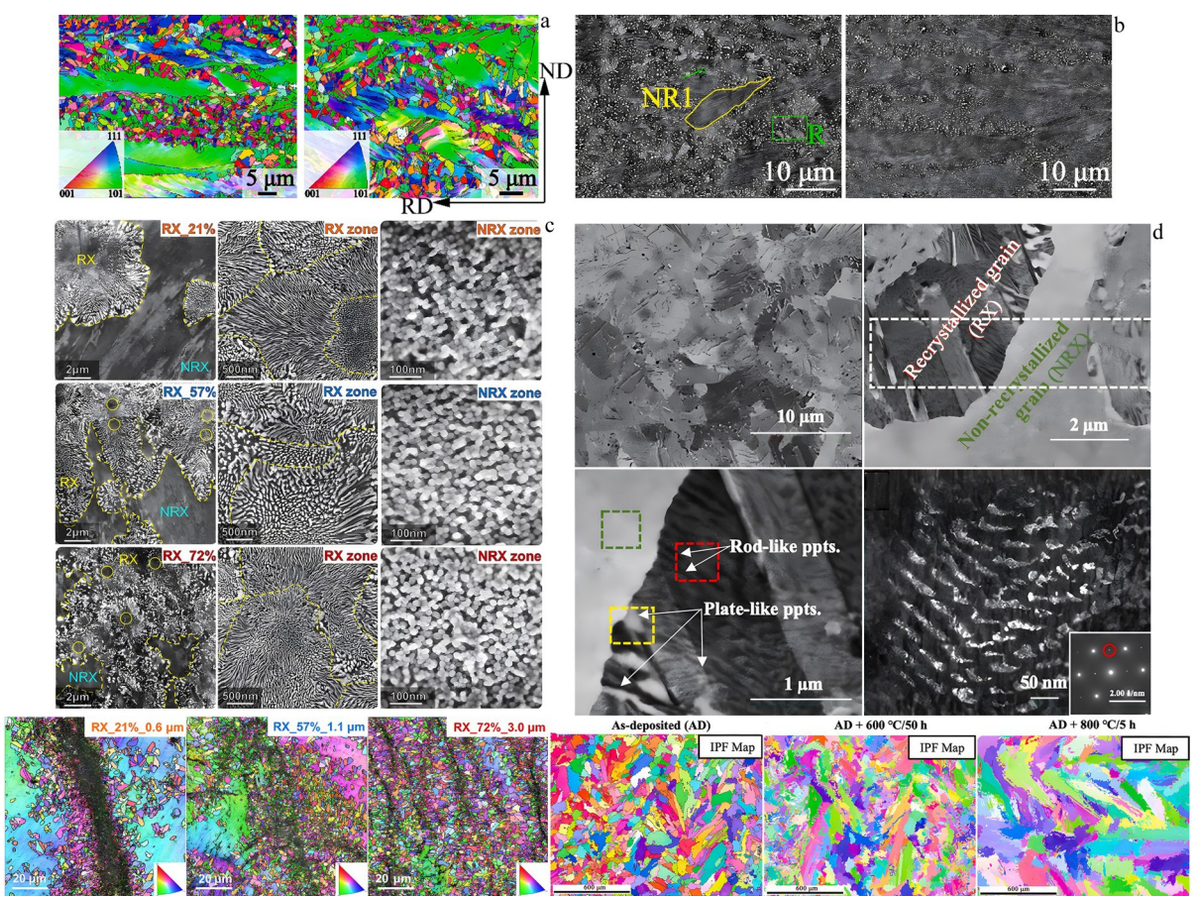

Fig.12 Hierarchical structures containing bimodal grain and massive phases[97,101,104]: (a) heterogeneous microstructures of $Al_{0.3}CoCrFeNi$ HEAs; (b) electron channeling contrast images of Fig. 12a; (c) heterogeneous microstructures of $Ni_2CoCrFeTi_{0.24}Al_{0.2}$ with different recrystallization volume fractions and grain sizes; (d) heterogeneous microstructures in $Al_{0.3}Ti_{0.2}Co_{0.7}CrFeNi_{1.7}$ HEA

fine (≤10 μm) and coarse (> 10 μm) heterogeneous grains and dual-phases located at the transitional region (close to 1 μm in thickness). Moreover, the combination of HDI hardening and precipitation hardening was jointly responsible for the optimized properties of the alloy[102]. A hierarchical heterostructure composed of grain and dual nanoprecipitates (B2 and $L1_2$) was introduced in a fcc $Al_{0.5}Cr_{0.9}FeNi_{2.5}V_{0.2}$ HEA[103]. The strength of the alloy was attributed to the HDI effects, as well as dislocation, GB strengthening, B2 nano-particles Orowan strengthening, $L1_2$ nanoparticles shearing strengthening and SRO strengthening[103]. Nartu et al[104] synthesized a novel hierarchically heterogeneous microstructure in $Al_{0.3}Ti_{0.2}Co_{0.7}CrFeNi_{1.7}$ HEA featured by heterogeneous grains with two different types of ordered nanoscale γ' and σ precipitates by AM (Fig. 11). The novel hierarchical heterostructures led to high YS close to 1150 MPa and moderate ductility[104].

2.2.3 Hierarchical heterogeneity composed of grains and defects

An interstitial HEA, $Fe_{49.5}Mn_{30}Co_{10}Cr_{10}C_{0.5}$, was prepared using the SLM process and resulted in the hierarchical heterostructure with length scales across several orders of magnitude and various defects[105]. The hierarchical heterostructure and high density of dislocations, DTs and phase transformations contributed to a high UTS of 1 GPa and the desired El. of approximately 28%[105]. Moreover, the SLM process was also used to modify the microstructure of an $AlCoCrFeNi_{2.1}$ EHEA[106] (Fig. 13). In Fig. 13, LNT means liquid nitrogen temperature. After the SLM process, a unique hierarchical heterostructure featuring ultrafine fcc and ordered bcc (B2) phases in the alloy and the duplex microstructure was transformed from a lamellar structure to a cellular structure owing to the decrease in laser energy input. Both the ultrafine grain (UFG) and heterostructures were responsible for the optimized performance of the alloy with a high UTS of 1271 MPa, YS of 966 MPa and good ductility of 22.5%[106]. A novel heterostructure containing UFGs at the nano/submicron scale, coarse grains, and hierarchical nanotwins was formed using various annealing temperatures and time in the CoCrFeMnNi HEA[107] (Fig. 12). The GND density and hierarchical nanotwins induced by the heterogeneous structure were primarily responsible for superior strain hardening, thus enhancing the overall performance of the alloy[107]. A multilayered heterostructure featuring fully recrystallized regions composed of coarse- and fine-grained regions and partially recrystallized regions was prepared using an ultrasonic nanocrystalline surface modification process[108]. The superior properties of the CoCrFeMnNi equiatomic HEA were attributed to deformation and grain size heterogeneity[108].

A combination of heterogeneous structures comprising nanotwins in the recrystallized grains, a high density of dislocations in the deformed regions and LRO Cr-rich precipitates was discovered in an equiatomic FeCrCoMnNi HEA processed by cold rolling, followed by isochronous annealing treatments[109]. A dual-heterogeneous structure encompassing both the grain size and dislocation heterogeneity was prepared in a metastable $Fe_{50}Mn_{30}Co_{10}Cr_{10}$ HEA by severe deformation at various annealing temperatures[110] (Fig. 12). The hierarchical heterostructure signifi-

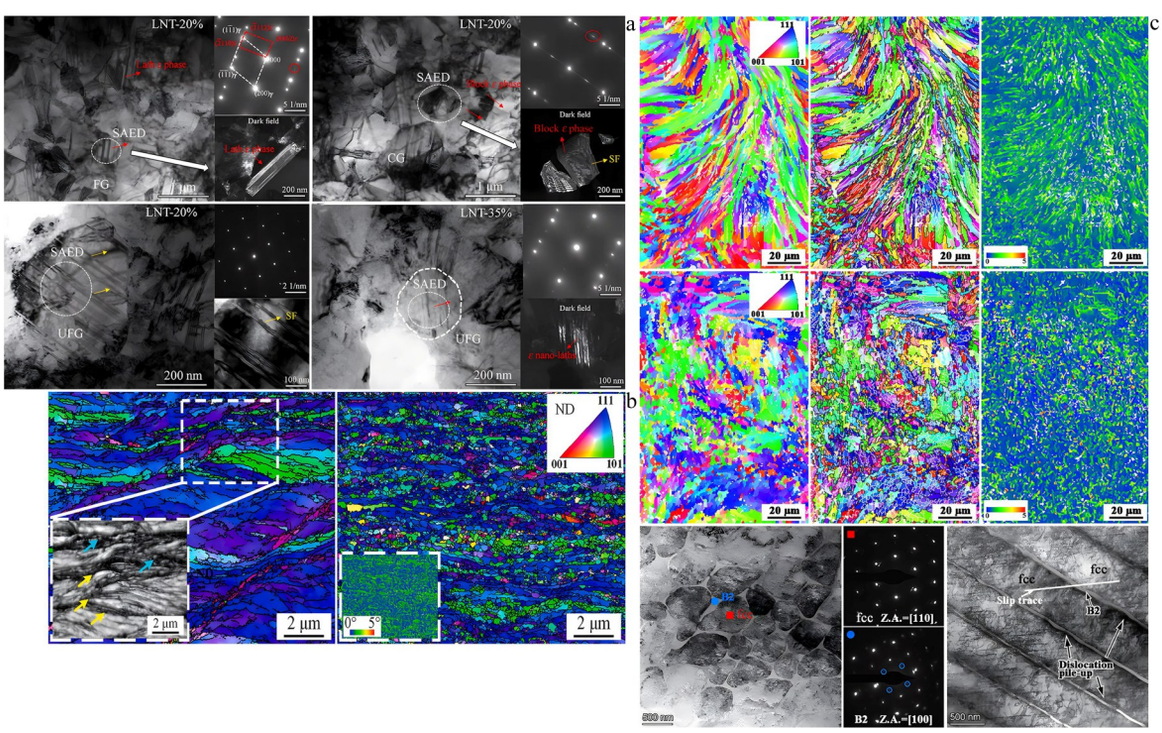

Fig.13 Hierarchical structures containing bimodal grains and massive defects[106–107,110]: (a) TEM images of deformed microstructure in HS-740 samples; (b) IPF maps and KAM maps of cold-rolled and annealed CoCrFeMnNi HEAs; (c) microstructures of SLMed $AlCoCrFeNi_{2.1}$ sample

cantly regulated the cryogenic mechanical performance of the alloy, resulting in a high YS of approximately 965 MPa, UTS of approximately 1680 MPa, and excellent El. of approximately 45%. The fundamental strengthening mechanisms of the alloy were the GB strengthening and dislocation strengthening, and high ductility originated from the hierarchical activation of TRIP and TWIP effects and train partitioning[110]. The addition of element N to a fcc FeCoNiCr HEA successfully activated heterogeneous hierarchical structures containing bimodal grain structures, low-angle boundaries and dislocation networks[111]. The N-doped HEA showed a good balance between strength and ductility owing to the strong strengthening effect and progressive strain hardening arising from the hierarchical heterogeneous structures[111]. Furthermore, cold rolling and partial recrystallization contributed to the formation of a trimodal heterostructure with DTs and dislocations, leading to a balance between strength and ductility in a CoCrFeNi HEA[112]. An et al[113] successfully prepared hierarchical heterogeneous twins in a $Co_{30}Cr_{20}Fe_{18}Mn_{18}Ni_{11}Si_3$ HEA using cold working. The hierarchical structure broke the strength-ductility trade-off of conventional metal alloys owing to the strain-hardening ability stemming from HDI hardening, TWIP and TRIP effects[113].

2.2.4 Hierarchical phase/precipitate heterogeneity

Chu et al[13] systematically studied the effects of diverse TMP on the formation of hierarchically heterogeneous phases in the $Al_{7.5}Co_{20.5}Fe_{24}Ni_{24}Cr_{24}$ HEA. They found that a desired hierarchical B2+$L1_2$+σ precipitate and a heterogeneous fcc matrix were easily formed after the transition from solid-solution annealing to recrystallization annealing. By contrast, the formations of the B2 and $L1_2$ phases were different. The former usually nucleated at defect-rich sites (deformation bands), and the latter was often homogeneously distributed in the fcc matrix[13]. The formation of the optimized hierarchical structure greatly contributed to superior properties at both room and liquid nitrogen (LN_2) temperatures, which mainly originated from DTs, HDI effects, SFs, SF-based substructures, L-C locks and the interaction among the optimized microstructures[13]. Yang et al[114] explored the influence of the annealing time on the microstructures and deformation mechanisms of a new fcc $Fe_{49.5}Mn_{30}Co_{10}Cr_{10}C_{0.2}Ti_{0.1}V_{0.1}Mo_{0.1}$ HEA. After cold rolling and annealing at 600 °C, a hierarchical precipitate structure was formed, including a σ-phase, Cr-rich MC-type carbides and nanoscale (Ti, V, Mo)C. The partially recrystallized microstructures and hierarchical precipitates were beneficial for the excellent YS, and the deformation mechanisms varied with annealing time[114]. After annealing for 10 h, the overall performance of the alloy included a YS of 699 MPa, UTS of 1041 MPa and El. of 45%, which primarily originated from various deformation mechanisms and high back stress strengthening[114]. An original hierarchical precipitate structure was observed in the as-cast $Fe_{27}Ni_{35}Cr_{18.25}Al_{13.75}Co_2Ti_2Mo_2$ HEA with ultrahigh tensile strength and excellent ductility[16] (Fig. 14). The hierarchical structure was characterized by an ultrafine lamellar microstructure (ULM), an ultrafine rhombus microstructure (URM), an ultrafine vermicular microstructure (UVM), nanosized precipitates and spinodal decomposition (SP), which resulted in a good balance of strength and ductility with a high YS of approximately 1056 MPa, UTS of approximately 1526 MPa and good El. of approximately 15.6%[16]. The excellent properties of the alloy are predominantly attributed to the desired HDI hardening and numerous interfaces[16].

Wang et al[4] discovered that hierarchical precipitate structures could significantly improve the strain-hardening ability of the $TiZrNbTaNi_{0.05}$ RHEA (MH-RHEA) via composition design and annealing. The tensile properties of the alloy were as follows: high YS of 1195±12 MPa, UTS of 1235±9 MPa and El. of 22.4±1.0%, which were primarily controlled by precipitation strengthening and HDI hardening[4]. A heterogeneous microstructure with multiscale precipitates ranging from nanoscale (<300 nm) and submicron (300–800 nm) to micron (>1 μm) in a bcc $(FeCr)_{45}(AlNi)_{50}Co_5$ HEA was prepared by the MA and SPS processes. The compressive properties of the alloy were significantly enhanced by reduced misfit strain at multiscale coherent precipitate interfaces[115]. Chen et al[116] effectively regulated the hard magnetic properties of the $Fe_2CoNiAlCu_{0.4}Ti_{0.4}$ HEA because of its hierarchically heterogeneous microstructure composed of chemical shape anisotropy and cellular nanostructure disordered bcc and $L2_1$ (ordered bcc) phases.

A complex two-hierarchy dual-phase structure was obtained in an $AlCoCrFeNi_{2.1}$ EHEA by laser powder bed fusion[117]. The two-hierarchy structure is characterized by a mixture of lamellar fcc and B2 nanoscale phases, as well as cellular structures including square fcc cells and surrounding B2 phases. The novel heterostructure contributed to the outstanding tensile properties of the alloy with a YS of 1042 MPa, UTS of 1303 MPa and El. of 26%[117]. The SLM process was also used to construct hierarchically heterogeneous microstructures comprising nanosized B2 and $L1_2$ phases, a cellular fcc matrix and Cr-rich clusters, contributing to ultrahigh strength (YS of 1446 MPa, UTS of 1737 MPa) and good ductility (El. of 11%)[118]. The TRIP and TWIP effects were introduced in a triphase heterogeneous $Al_9(Fe_{50}Mn_{30}Co_{10}Cr_{10})_{91}$ HEA, overcoming the strength-ductility trade-off[119]. After a reasonable TMP process, the hierarchical microstructure of fcc, bcc and a small number of hcp phases favored the desired properties[119]. Fig. 15 shows the hierarchical structures composed of multiple phases or precipitates, and Fig. 16 shows a schematic diagram of the hierarchical microstructure composed of different phases or precipitates.

3 Heterogeneous Structures in MEAs

3.1 Regulation of single heterogeneity for MEA performance

It is known that MEA is another promising metallic material for industrial applications due to its superior comprehensive performance[20]. Moreover, it will availably improve the performance of MEAs by reasonably regulating

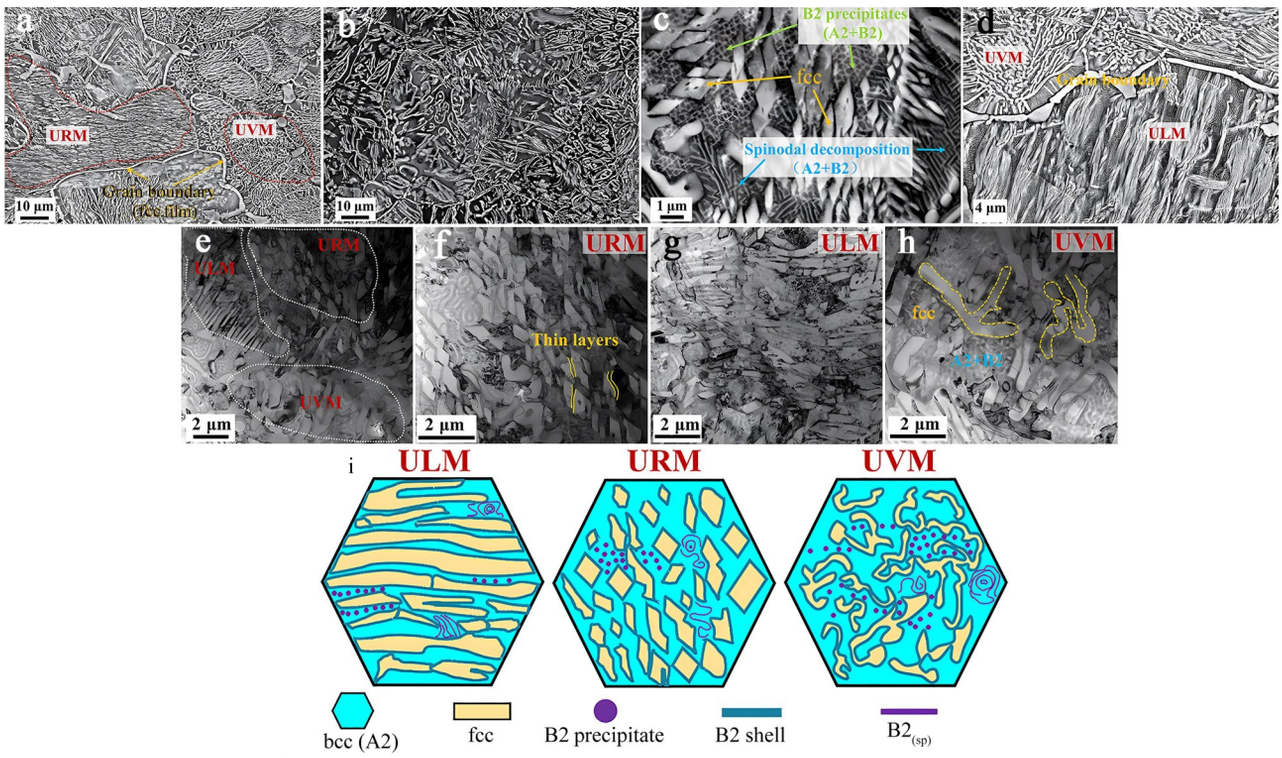

Fig.14 Hierarchical microstructure containing URM, UVM and ULM in as-cast $Fe_{27}Ni_{35}Cr_{18.25}Al_{13.75}Co_2Ti_2Mo_2$ HEA: (a) BSE image of URM and UVM; (b) BSE image of hierarchical microstructure with different morphologies within a grain; (c) high-magnification BSE image of UVM; (d) BSE image of ULM; (e–h) TEM images and (i) schematic diagrams of ULM, URM and UVM[16]

their microstructures, such as multiple dislocation slips, DTs, SFs, L-C locks, S/M/LRO structures, abundant substructures, etc[15]. More importantly, similar to that of HEA, regulating heterostructures is an anticipated strategy for enhancing overall properties of MEAs. The heterostructures in MEAs also consist of single and hierarchical heterogeneities. In this section, the effect of single heterogeneity on the microstructure evolution and performance regulation of MEAs was basically discussed.

3.1.1 Bimodal structure

The bimodal structure is a vital heterostructure for improving performance and regulating microstructures of MEAs. Herein, the microstructure evolution and deformation mechanisms of bimodal structure constructed by various rolling processes in MEAs were explored and discussed.

(1) Cold-rolling process and corresponding heat treatments

It has been reported that fcc/bcc MEAs constantly suffer the strength-ductility trade-off dilemma[6]. Gu et al[20] developed single-phase fcc $Ni_2CoFeV_{0.5}$ MEAs with a typical heterostructure featuring recrystallized micro-grain lamellae and non-recrystallized nano-/ultrafine-grain lamellae induced by cold rolling followed by annealing. The bimodal heterogeneous lamellar (HL) structure significantly improved the tensile properties of the alloys with a high YS of 1120 MPa and El. of 12.3%. The origin of the high performance was HDI strengthening and the notable Hall-Petch effect, controlled by the high density of twins and GBs[20]. A heterogeneous ultrafine-grained CrCoNi MEA was prepared using cold rolling and short-term annealing to enhance its strength and ductility[120]. A HGS coupled with nanoscale precipitates and twins effectively optimized the cryogenic YS and uniform El. of the $Al_{0.3}$CoCrNi alloy, which is attributed to the nanoscale DTs, HDI strain and the interaction between dislocations and B2 precipitates in the DTs MEA[121]. A high-performance $Co_{36}Ni_{36}Cr_{20}Al_3Ti_2Nb_3$ MEA was prepared by cold rolling and annealing, characterized by a HGS and the block and lamellar η^*-Ni_6(Al, Ti)Nb phases[122].

The effect of element Ta addition on the mechanical properties of a CoCrNi-AlTi MEA was studied. After cold rolling and the corresponding heat-treatment process, a complex microstructure consisting of heterogeneous incompletely recrystallized grains and nanoscale lamellar precipitates was observed in the alloy, leading to a high YS of 1385 MPa, UTS of 1690 MPa and moderate El. of 7.44%[123]. Peng et al[124] explored the effects of both aging temperature and element V addition on the microstructure regulation and performance enhancement of $Ni_{43.4}Co_{25.3}Cr_{25.3}Al_3Ti_3$ MEA. The results showed that HGS composed of fine soft recrystallized grains and hard large deformed grains was formed and the heterostructure validly optimized the mechanical properties of the alloy at room and cryogenic temperatures owing to back-stress hardening, Hall-Petch strengthening and dislocation hardening[124]. Cold rolling and annealing were conducted to regulate the microstructure and performance of a single-phase equiatomic CrCoNi MEA[125]. Heterogeneous and partially recrystallized microstructures were constructed using a rolling

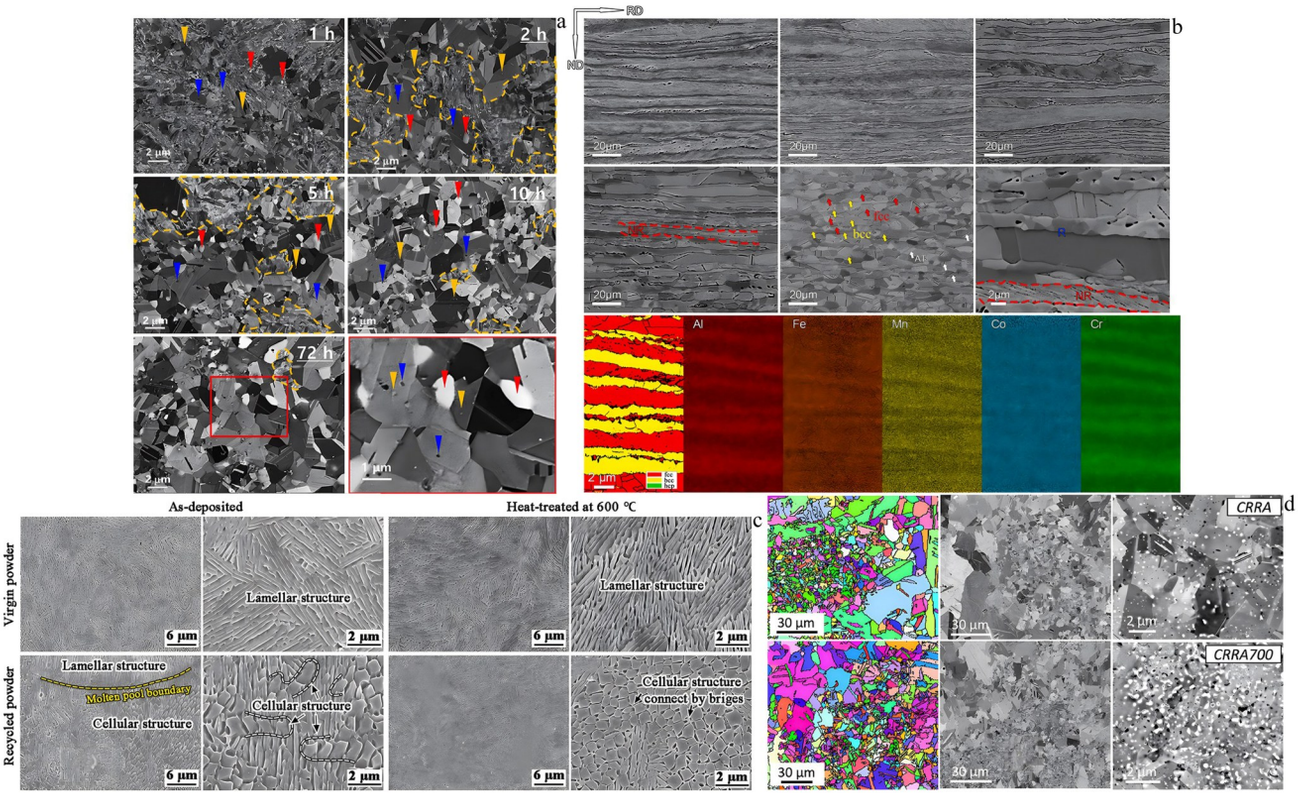

Fig.15 Hierarchical structures composed of multiple phases or precipitates[13,114,117,119]: (a) materials annealed for different time; (b) SEM images of cold-rolled and annealed samples, EBSD images and EDS maps of sample annealed at 1173 K; (c) different phase structures; (d) EBSD and SEM images of grains and precipitates

process to obtain a superior combination of YS (approximately 1100 MPa) and ductility (El. of approximately 23%) [125]. Moreover, bimodal heterostructures were also prepared by cold rolling and the corresponding heat-treatment process to significantly improve the overall performance of MEAs, such as CoCrNiSi[126], equiatomic CrCoNi[120,127] and $Al_{0.3}$CoCrNi[128]. In these MEAs, a combination of heterostructures and specific microstructures is responsible for their enhanced properties, and the primary deformation mechanisms are HDI strengthening and hardening[120,126–127].

To introduce a heterogeneous dual-grain structure, a combination of hot-forging and cold-rolling processes was conducted[23]. After the deformation process, dual gradients of grain size and coherent $L1_2$ nanoprecipitation were observed in the $Co_{34.46}Cr_{32.12}Ni_{27.42}Al_3Ti_3$ MEA, and abundant DTs and SFs were discovered in the alloy because of the grain-size gradient structure. Moreover, high strain-hardening ability was obtained for the alloy owing to HDI hardening and strong precipitation hardening originating from the interaction between the DTs and $L1_2$ phases, which improved the tensile ductility of the alloy[23]. However, both hot-forging and cold-rolling processes induced a heterogeneous dual structure consisting of deformed substructures (the hard zone) and recrystallized ultrafine/fine grains (the soft zone) in the CrCoNi MEA[24]. The cryogenic tensile properties of the alloy were significantly enhanced by the high back stress and strain hardening introduced by the heterostructures and tailored microstructures, respectively[24]. A combination of hot-forging and cold-rolling processes was also used to regulate the microstructure of the $(CoCrNi)_{94}Al_4Ti_2$ MEA[19]. Surprisingly, a HGS with coherent $L1_2$ nanoprecipitates was formed in the alloy via deformation. Meanwhile, the shearing of the $L1_2$ phases by dislocations can induce high HDI stress and work hardening owing to the superior ductility of the alloy. Moreover, SFs, L-C locks and 9R structures were observed in the alloy after tensile deformation, leading to enhanced strain hardening and improved alloy properties[19]. A novel $CrCoNiN_{1.75}$ MEA was prepared via hot forging and cold rolling to obtain a HGS, which helped to optimize the fracture toughness and YS of the alloy owing to its superior strain-hardening ability[21].

(2) Cryogenic rolling process and corresponding heat treatments

Cryogenic rolling and annealing were used to regulate the microstructure of a $Cr_{15}Fe_{55}Mn_{20}Ni_{10}$ ferrous MEA. Substantial shear bands, deformation-induced martensite and residual matrix were obtained after cryogenic rolling[129]. More importantly, heterogeneous microstructures with multiscale grains were introduced into the alloy after short-term annealing following cryogenic rolling, resulting in good strength and ductility. The enhanced properties of the alloy originated mainly from GB, HDI and dislocation

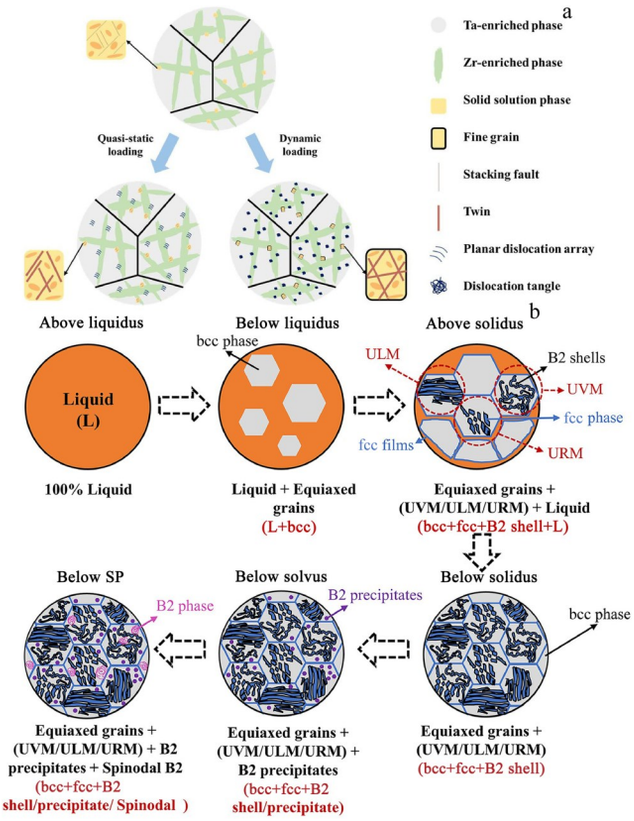

Fig.16 Schematic diagrams of hierarchical microstructure composed of different phases or precipitates in TiZrNbTaNi HEA (a)[4] and as-cast $Fe_{27}Ni_{35}Cr_{18.25}Al_{13.75}Co_2Ti_2Mo_2$ HEA (b)[16]

hardening[129]. Furthermore, a heterostructure composed of fine and coarse grains decorated with nanometric precipitates was obtained by cryogenic rolling and annealing, followed by aging[130]. The properties of the alloy at room and cryogenic temperatures were optimized because of the appearance of heterogeneous bimodal grain structures, which provided beneficial HDI strengthening[130].

(3) Other techniques for preparing bimodal structure

AM is another available process method to prepare bimodal structure in MEAs. Ahn et al[22] developed a new NiCoCrC MEA by using a powder bed fusion. The results showed that the addition of element C into NiCoCr MEA was beneficial to the formation of a HGS. Meanwhile, there were a large number of nanosized precipitates, SFs and DTs in the alloy. Both the HGSs and specific microstructures could improve strain hardening and ductility[22].

3.1.2 Dual-phase structure

Dual-phase structure is another prominent heterostructures for optimizing performance of MEAs. There exist some advanced techniques for preparing dual-phase structure in MEAs, and the rolling process is also the most popular and effective method for preparing heterogeneous dual-phases (Fig.17).

Moon et al[131] proposed a new strategy for developing a lightweight $Al_x(CuFeMn)_{100-x}$ MEA with excellent mechanical properties. The results showed that after cold rolling and annealing, the microstructure of the MEA was sensibly regulated, and heterogeneous fcc and bcc dual phases were formed in the alloy. The high strength of the alloy stemmed from solid solution strengthening and HDI strengthening[131]. A combination of heterostructures and deformation-induced martensitic transformation (DIMT) was induced in a $Fe_{60}Co_{15}Ni_{15}Cr_{10}$ Fe HEA by cold rolling and subsequent short-term annealing[132]. The bcc phases were introduced into the alloy by pre-straining and subsequently transformed into fcc phases (reverse martensitic transformation) owing to the annealing treatment, resulting in a bimodal fcc hetero-structure[132]. A FeCrNiCoAl MEA was developed, and its microstructure and properties were regulated by cold rolling and a subsequent annealing process[133]. Dual-phase structures consisting of the Fe-Cr-Ni-rich fcc phase and Ni-Al-rich bcc phase were responsible for the optimized properties at room and cryogenic temperatures owing to DIMT and HDI hard-ening[133]. A dual-phase structure was induced in a non-equiatomic $Ni_{46}Co_{24}Fe_{24}Al_3Ti_3$ MEA via cold rolling and subsequent heat treatment[134]. A heterogeneous phase structure composed of fcc matrix and short-rod $L1_2$ phase was formed by discontinuous precipitation (DP) and continuous precipitation (CP). Both the soft fcc matrix and the hard $L1_2$ precipitates contributed to the superior performance of the alloy[134]. Additionally, a dual-phase structure was prepared by cold rolling, followed by heat treatment of $Fe_{65}Ni_{15}Cr_{10}Co_{10}$[135] and $(CoCrNi)_{93}Mo_7$ MEAs[136].

A hot-rolling process was also proposed to regulate the microstructure of a $(NiCoCr)_{88}Al_{10}Ta_2$ MEA and to improve its properties owing to the formation of dual-phases featuring the fcc matrix and B2 phases[137]. The properties of the alloy were as follows: YS of approximately 1.1 GPa, UTS of 1.4 GPa and El. of 20% at room temperature, YS of approximately 1.5 GPa, UTS of 1.8 GPa and El of 25% at cryogenic temper-ature, which remarkably originated from the B2 hardening, cooperation of planar slip, SF, and twinning mediated by the heterogeneous phase structures[137]. The properties of the $(Fe_{50}Mn_{25}Ni_{10}Cr_{15})_{100-x}Al_x$ MEA were dramatically enhanced by rolling at room temperature followed by annealing[138]. The process, accompanied by a variation in Al content, successfully formed the fcc and bcc dual-phase, leading to a high UTS of 1077 MPa and El. of approximately 85% at cryogenic temperature due to the solid solution strengthening, HDI strengthening and TWIP effect[138].

3.2 Regulation of hierarchical heterogeneity for MEA performance

The hierarchical heterogeneity is a noteworthy strategy for optimizing performance of MEAs. The typical hierarchical heterostructures contain gradient microstructure bimodal grain coupled with some specific phases or defects and some hierarchical structures, which can effectively regulate MEA microstructure via peculiar defects and provide extra hardening and strengthening mechanisms to enhance MEA performance. Therefore, regulating hierarchical heterostruc-tures and exploring corresponding contribution for micro-structure and performance of MEA is a promising approach

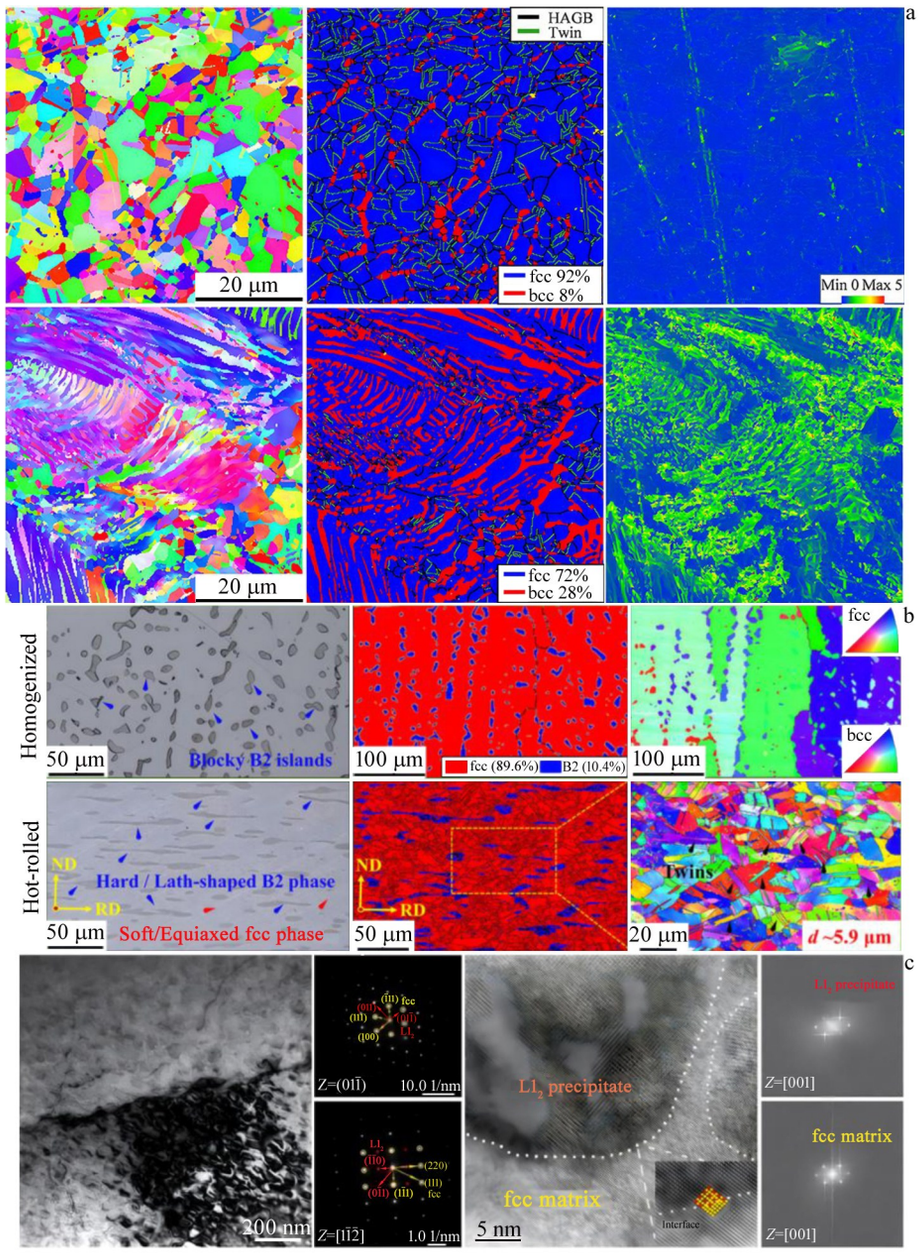

Fig.17 Dual-phase structures in different MEAs: (a) EBSD results of dual-phase[134]; (b) microstructure of different treatment process in MEA[137]; (c) TEM images of as-cast $Ni_{46}Co_{24}Fe_{24}Al_3Ti_3$ MEA[138]

for modifying overall properties of MEAs.

3.2.1 Gradient structure

The high energy shot peening process has been used to successfully construct the gradient nanograined (GNG) structure in the CrCoNi MEA, containing a gradient distribution of grain size from nanometer (approximately 50 nm) to micrometer (approximately 1.3 μm) at the center layer[139]. The GNG structure remarkably regulated performance of the alloy, which included a desired YS of approximately 1215 MPa, UTS of approximately 1524 MPa and considerable El. of approximately 23%, achieving a balance between strength and ductility of the alloy. The potential HDI strengthening and hardening favored strength enhancement, excellent ductility and strain hardening capacity[139]. Moreover, an ultrasonic surface rolling process (USRP) was implemented on AM-prepared $(CoCrNi)_{94}Al_3Ti_3$ MEA, contributing to the formation of a gradient nanostructure[13]. The cryogenic properties of the alloy were notably enhanced and obtained an ideal YS of 1274 MPa and high ductility of 24.6%. Both the AM and USRP processes were advantageous for achieving a high YS owing to HDDs formed in the processes. The desired ductility of the alloys was attributed to HDI hardening and activated twinning/microband behavior[13]. A hot-forged cold-rolling process also facilitated the formation of a three-level HGS with grain sizes ranging from nanometers to micrometers[140]. The hierarchical heterostructures resulted primarily from the low SFE of the alloy, leading to the activation of massive SFs and DTs. The

heterostructure imparted an excellent YS over 1 GPa and favorable tensile strain of 22%, which mainly resulted from high back stress[140]. On the other hand, the USRP similarly initiated a HGS in a CrCoNi MEA, achieving an ultrahigh ductility of 54.1% induced by the HGS and abundant nanoscale DTs[141].

3.2.2 Hierarchical heterogeneity composed of grains and optimized microstructures

Hierarchical heterostructures were designed to overcome the trade-off between strength and ductility in a $Co_{30}Cr_{20}Ni_{40}$-V_5Ta_5 MEA[25] (Fig. 17). The low SFE matrix, numerous $D0_{22}$-γ'' nanoprecipitates, shearable and non-shearable intermetallic particles, and HGS are associated with hierarchical heterostructures and could provide cross-scale and dynamic strain partitioning to strengthen the alloy and obtain a high strain-hardening ability, finally leading to a superior YS of 1323 MPa, UTS of 1690 MPa and El. of 29%[25]. Dual heterostructures comprising a bimodal grain structure of fine and coarse grains and $L1_2$ phases with sizes ranging from the submicron to nanoscale were prepared in a novel non-equiatomic $Ni_{40}Co_{30}Cr_{20}Al_5Ti_5$ MEA[142] (Fig. 17). The tensile properties of the alloy were remarkably enhanced, yielding a high YS of 1200 MPa, a UTS of 1560 MPa and total El. of 33.6%. Multiple strengthening mechanisms, including HDI strengthening, GB strengthening and precipitation strengthening, were responsible for the superior strength and regulated microstructures containing high-density SFs and L-C locks, which contributed to the desired ductility[142]. A novel Co-free non-equiatomic $Ni_{46}Cr_{23}Fe_{23}A_{l4}Ti_4$ MEA was developed using multi-pass cold rolling following a heat-treatment process, which induced dual heterostructures consisting of three-level grain structures and heterogeneous $L1_2$ precipitates[143]. The specific hierarchical structures contributed to excellent strength-ductility synergy, with a high YS of approximately 1203 MPa, UTS of approximately 1633 MPa and El. of approximately 28.7%, resulting from HDI strengthening and hardening, the formation of SFs networks, numerous L-C locks and precipitate hardening[143].

Chou et al[144] prepared a $Co_{40}Cr_{20}Ni_{30}Al_5Ti_5$ MEA based on hetero-grain/precipitation engineering to overcome the temperature-dependent embrittlement of many structural materials. The heterostructures contained partial recrystallization structures and $L1_2$ nanoprecipitates, enhancing the performance, and especially the ductility, of the alloy at −196 °C and elevated temperatures up to 700 °C. The superior performance over a wide range of temperature results from stable deformed grains and pronounced planar defects, including SF networks and deformation twins[144]. To overcome the limitation of low YS in a CoCrNi alloy, a combination of the heterogeneous grains caused by the heterogeneous precipitates and element Ta doping was implemented to achieve a high-performance $(CoCrNi)_{98}Ta_2$ MEA with the desired YS of approximately 1200 MPa, UTS of approximately 1500 MPa and high ductility of approximately 33%[145]. These exceptional comprehensive properties were ascribed to the HDI hardening and numerous DTs[146]. The refined hierarchical microstructures characterized by coarse grains with an average size of 30 μm, UFGs with an average size of 1 μm and the heritage of dislocation-formed subgrains and other lattice defects were successfully introduced in a CoCrNi MEA by SLM followed by cold-rolling and annealing processes[145] (Fig. 17). A balance of strength and ductility of the alloy was achieved after the process, which was YS of 693.4 MPa, UTS of 912.7 MPa and El. of 31.5%. The exceptional performance resulted from hierarchical and regulated microstructures, such as annealing twins and lattice defects[145]. The dual heterostructures of a partial recrystallization matrix and heterogeneous nano-precipitates were significantly helpful in the performance enhancement of a novel $(Fe_{65}Ni_{15}Cr_{10}Co_{10})_{92}Ti_5Al_3$ MEA resulting from HDI strengthening, precipitation strengthening and the fcc→bcc martensitic TRIP effect[147].

A high-performance $(CoCrNi)_{94}Al_3Ti_3$ MEA with a remarkable hierarchical heterostructure characterized by a heterogeneous grain size, cellular substructure and characteristics of nanoprecipitates ($L1_2$ phase) had ideal tensile strength-ductility combinations at room and cryogenic temperature after AM and age hardening[148]. The excellent strength mainly resulted from HDI strengthening, and the good ductility was ascribed to HDI hardening, the precipitate shearing mechanism and deformation-induced SF-based substructure[148]. Moreover, a combination of hot and cryogenic rolling following a reasonable heat-treatment process was implemented for a $Co_{34.46}Cr_{32.12}Ni_{27.42}Al_3Ti_3$ MEA, facilitating the formation of a typical hierarchical heterostructure of both matrix with coarse grains (10–30 μm), UFGs (0.5–2.0 μm) and precipitates featured by fully coherent heterogeneous $L1_2$ nanoprecipitates[149] (Fig. 18). The distinct comprehensive properties of the alloy were imparted because of the HDI effect and the minimum elastic misfit strain of the interfaces owing to the full coherence between the matrix and $L1_2$ nanoprecipitates[149]. Hot forging and cold rolling processes were also implemented on a $Co_{34.5}Cr_{32}Ni_{27.5}Al_3Ti_3$ MEA, resulting in dualheterogeneous structures with both HGSs and coherent $L1_2$ nanoprecipitates[150]. Heterogeneous structures and optimized microstructures consisting of DTs, SFs and L-C locks are responsible for the performance enhancement of the alloy[150]. In addition, a hierarchically heterogeneous microstructure with various sizes contributed significantly to the performance of a metastable dual-phase $Fe_{59}Cr_{13}Ni_{18}Al_{10}$ MEA owing to numerous deformation mechanisms, including fine grains, dislocations, precipitation, transformation-induced plasticity, SFs and nanotwins[151].

3.2.3 Other specific hierarchical heterogeneity

A hierarchical heterogeneity existing in HDD formed cellular structures and low-angle grain boundaries (LAGBs) within the heterogeneous columnar grains was achieved in a fully-dense CrCoNi MEA by the SLM process, which resulted in a high UTS of 1340 MPa and reasonable ductility of 47% at 77K[152]. A novel metastable maraging $Fe_{68}Ni_{10}Mn_{10}Co_{10}Ti_{1.5}Si_{0.5}$

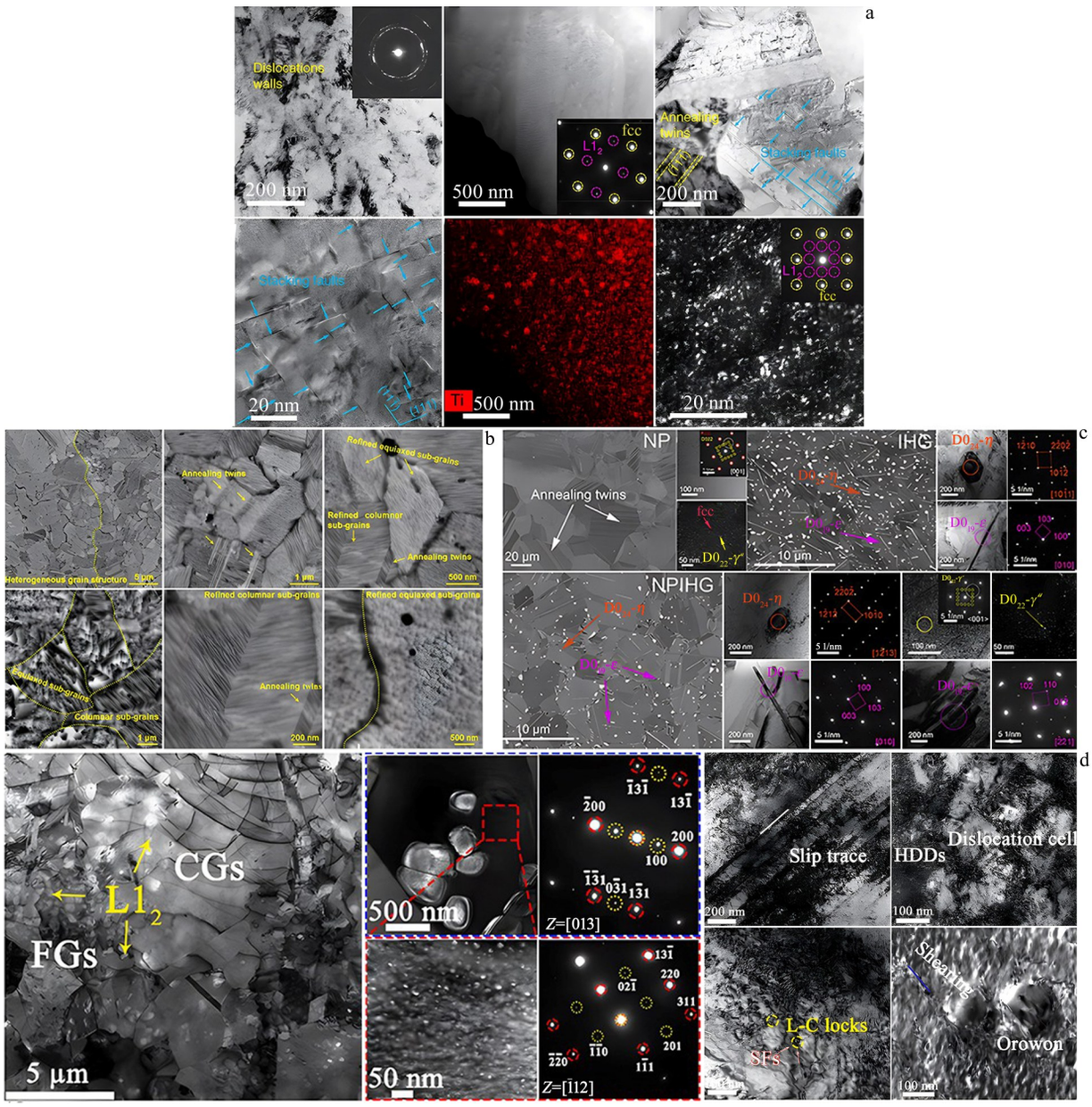

Fig.18 Hierarchical structures containing bimodal grain and a large number of phases or precipitates[25,142,145,149]: (a) microstructures of Co-Cr-Ni MEA; (b–d) different phases in MEAs

MEA with hierarchical heterogeneity was prepared based on the concept of maraging characteristics[153]. The hierarchical heterostructures contained a dual-phase microstructure, compositional gradient heterogeneity and nanoprecipitates enhanced by $(NiMn)_{3-x}Ti_x$ and η-Ni_3Ti phases, which contributed to an ultrahigh YS of approximately 1.3 GPa and desired El. of approximately 25.3%, resulting from HDI strengthening and DIMT effect[153]. Various heterogeneities were obtained via a laser-based DED, including the formation of HGSs, dual-phase structure, in situ formed η nanoprecipitate, cellular structure and elemental segregation[154]. Several strengthening mechanisms contributed to the high strength at room and cryogenic temperatures, such as HDI strengthening precipitation/SF strengthening, deformation-induced martensite transformation from fcc to bcc, solid solution strengthening and other optimized microstructure contributions[154]. Furthermore, a multiscale heterogeneous structure was introduced into the $(CoCrNi)_{94}Ti_3Al_3$ MEA for enhancing its properties, with a superior UTS of 1.6 GPa and El. of 13.1%[155]. The hierarchical heterogeneity was composed of fcc matrix, coherent γ' nanoprecipitates and numerous crystalline defects, such as dislocations, small SFs, L-C locks, and ultrafine nanotwins, resulting in the superior performance of the alloy[155–156].

4 Conclusions

1) Compared to traditional homogeneous microstructures, heterostructures can be significantly changed to regulate the properties and microstructures of HEAs. Many heterogeneities

have been introduced into HEAs, including compositional inhomogeneity, bimodal structures, dual-phase structures, lamella/layered structures, HS (core-shell), multiscale precipitates and heterostructures coupled with specific microstructures. The primary strategy of regulating single heterogeneous structures involves various rolling processes followed by advanced heat-treatment processes, which include reasonable alloy doping, powder metallurgy, AM, hot-forging processes, and FSW. The formation of single heterogeneous structures significantly facilitates different properties of HEAs via the superior HDI effect and multiple mechanisms introduced by the optimized microstructures.

2) Recently, specific hierarchical heterogeneity has been imparted to HEAs to optimize their performance. Hierarchical heterostructures are characterized by gradient microstructures, bimodal grains coupled with specific defects or phases and hierarchically heterogeneous phases. There are many advanced techniques for designing hierarchical heterogeneous structures in HEAs, such as RASP, SMAT, laser surface remelting, multiple-stage heavy drawing, UNSM, multiple rolling processes, spray-granulated powder, HPT, AM, reasonable alloying design and heat treatment. Hierarchical heterogeneity significantly regulated the overall performance of the HEAs via a more effective HDI effect than other single heterostructures. More importantly, many optimized microstructures appear in HEAs after the treatments, such as multiple dislocation slips, heterogeneous defects (SFs, DTs with various sizes and morphologies, dislocation cells and abundant substructures), L-C locks, 9R/6R structures, S/M/LRO structures, highly coherent $L1_2$ phase, B2 strengthening phase, nanoprecipitates, heterogeneous nanoparticles and ultrafine phases with different morphologies. The strong HDI effect and abundant optimized microstructures can provide additional mechanisms for optimizing the comprehensive properties of HEAs and facilitate their industrial applications.

3) Similar to those in the HEAs, single and hierarchical heterogeneities are successfully constructed in MEAs. Both single and hierarchical heterogeneous structures can effectively optimize the overall performance of MEAs, especially their mechanical properties. Single heterogeneous structures in MEAs include a bimodal structure, primarily regulated by various rolling processes, and a dual-phase structure. The hierarchical heterogeneities of MEAs are composed of a gradient structure, grains, optimized microstructures and other specific hierarchical heterogeneities. Furthermore, a combination of the HDI effect and multiple deformation mechanisms induced by various optimized microstructures is achieved in MEAs, resulting in a balance between strength and ductility.

5 Outlook

Diverse techniques exist for constructing single and hierarchical heterogeneous structures in H/MEAs, particularly in massive rolling processes. Some SPD processes, such as SMAT, surface mechanical grinding treatment, surface mechanical rolling treatment, laser shock processing, shot peening, HPT and equal-channel angular pressing, inherently help the formation of heterostructures owing to the tremendous and gradient strain distribution, resulting in the desired heterogeneity. Accordingly, a combination of SPD process, reasonable heat-treatment techniques and traditional deformation techniques, including rolling, forging, extrusion, drawing, AM and MA+SPS, is a promising strategy for effectively building heterostructures in H/MEAs.

Hierarchical heterogeneous structures have been seen as more beneficial approaches for optimizing the comprehensive properties of H/MEAs owing to multiple HDI effects. A composite of multiple heterogeneous structures, such as mixtures of grains and twins, grains and defects, grains and precipitates and twins and precipitates, is an effective method for improving the properties of H/MEAs.

Furthermore, optimized microstructures can significantly optimize the overall performance of H/MEAs. Consequently, a combination of single/hierarchical heterogeneous structures and advantageous microstructures, such as SFs or DTs with various sizes and morphologies, dislocation cells, abundant substructures, L-C locks, 9R/6R structures, S/M/LRO structures, highly coherent $L1_2$ phases, B2 strengthening phases, nanoprecipitates, heterogeneous nanoparticles and ultrafine phases with different morphologies, is a noteworthy mean of developing high-performance H/MEAs.

References

1 Huang E W, Lee W J, Singh S S *et al*. *Materials Science and Engineering R*[J], 2022, 147: 100645

2 Qin S, Yang M X, Jiang P *et al*. *Acta Materialia*[J], 2022, 230: 117847

3 Lu W J, Guo W Q, Wang Z W *et al*. *Acta Materialia*[J], 2023, 246: 118717

4 Wang R X, Tang Y, Ai Y L *et al*. *International Journal of Plasticity*[J], 2024, 173: 103882

5 Guo H X, Wang J J, Tu X X *et al*. *Journal of Materials Research & Technology*[J], 2024, 28: 3093

6 Mishra R S, Haridas R S, Agrawal P. *Materials Science and Engineering A*[J], 2021, 812: 141085

7 Pan Q S, Zhang L X, Feng R. *Science*[J], 2021, 374(6570): 984

8 Han D, Cai S X, Sun W H et al. *Advanced Engineering Materials*[J], 2023, 25: 2300291

9 Chen H X, He Y X, Dash S S *et al*. *Materials Research Letters*[J], 2024, 12(3): 149

10 Wu Y Q, Liaw P K, Li R X *et al*. *International Journal of Minerals Metallurgy and Materials*[J], 2024, 31: 1350

11 Yu B X, Ren Y S, Zeng Y et al. *Journal of Materials Research & Technology*[J], 2024, 29: 2689

12 Chen F, Liu F, Tan Y B *et al*. *Journal of Materials Research & Technology*[J], 2024, 29: 265

13 Chu C L, Chen W P, Huang L R *et al*. *International Journal of Plasticity*[J], 2024, 175: 103939

14 Sui Q X, Wang Z, Wang J *et al*. *Journal of Materials Research*

& Technology[J], 2024, 30: 1992
15 Wang X D, Zhang Z, Wang Z B *et al*. *Materials*[J], 2022, 15(3): 1215
16 Niu J C, Fu Z Q, Chen W P *et al*. *Journal of Materials Science & Technology*[J], 2024, 179: 9
17 Wu Xiaolei, Zhu Yuntian. *Acta Metallurgica Sincia*[J], 2022, 58(11): 1349 (in Chinese)
18 Wu X L, Yang M X, Li R G *et al*. *Science China Materials*[J], 2021, 64(6): 1534
19 Zhang Z H, Ma Y, Yang M X *et al*. *International Journal of Plasticity*[J], 2024, 172: 103821
20 Gu L, Hou R, Liu Y *et al*. *Journal of Materials Science & Technology*[J], 2023, 151: 19
21 Liu X R, Zhang S D, Feng H *et al*. *Acta Materialia*[J], 2023, 255: 119079
22 Ahn J E, Kim Y K, Yang S *et al*. *Journal of Alloys and Compounds*[J], 2022, 918: 165601.
23 Zhang Z H, Wu X L, Yuan F P. *Materials Characterization*[J], 2023, 205: 113372
24 Guo F J, Song L Y, He Q *et al*. *Materials Characterization*[J], 2023, 201: 112951
25 Guo S K, Ma Z, Xia G H *et al*. *Acta Materialia*[J], 2024, 263: 119492
26 Guo L, Gu J, Gong X *et al*. *Micron*[J], 2019, 126(7777): 102739
27 Ding Q Q, Zhang Y, Chen X *et al*. *Nature*[J], 2019, 574(7777): 223
28 Bu Y Q, Wu Y, Lei Z F *et al*. *Materials Today*[J], 2021, 46: 28
29 Hu Q, Guo S, Guo J L *et al*. *Journal of Alloys and Compounds*[J], 2022, 906: 164186
30 Lei Z F, Liu X J, Wu Y *et al*. *Nature*[J], 2019, 565(7732): E8
31 Zhang J, Yoon K N, Kim M S *et al*. *Metals*[J], 2021, 11(9): 1487
32 Rizi M S, Minouei H, Lee B J *et al*. *Materials Science and Engineering A*[J], 2021, 824: 141803
33 Li Q J, Sheng H, Ma E. *Nature Communication*[J], 2019, 10: 3563
34 Zhang R P, Zhao S T, Ding J. *Nature*[J], 2020, 581(7808): 283
35 Su I A, Tseng K K, Yeh J W *et al*. *Scripta Materialia*[J], 2022, 206: 114225
36 Chen X F, Wang Q, Cheng Z Y *et al*. *Nature*[J], 2021, 592(7856): 712
37 Wang J, Jiang P, Yuan F P *et al*. *Nature Communication*[J], 2022, 13: 1021
38 Chen T, Chen W P, Wu R J *et al*. *Materials Today Communications*[J], 2023, 35: 106150
39 Xie Y H, Liang J M, Zhang D L *et al*. *Scripta Materialia*[J], 2020, 187: 390
40 Fu Z Q, MacDonald B E, Dupuy A D *et al*. *Applied Materials Today*[J], 2019, 15: 590
41 Borujeni A M, Shahmir H, Shams S A A *et al*. *Materials Science and Engineering A*[J], 2024, 898: 146397
42 Wu S W, Wang G, Wang Q *et al*. *Acta Materialia*[J], 2019, 165: 444
43 Wu Y T, Jin X, Zhang M *et al*. *Materials Today Communications*[J], 2021, 28: 102718
44 Du Y J, Xu S M, Wang F *et al*. *Journal of Alloys and Compounds*[J], 2024, 993: 174550
45 Shukla S, Choudhuri D, Wang T H *et al*. *Materials Research Letters*[J], 2018, 6(12): 676
46 An Z B, Mao S C, Liu Y N *et al*. *Acta Materialia*[J], 2023, 243: 118516
47 He F, Yang Z S, Liu S F. *International Journal of Plasticity*[J], 2021, 144: 103022
48 Man J L, Wu B L, Duan G S *et al*. *Materials Science and Engineering A*[J], 2022, 858: 144137
49 Wu B L, Man J L, Duan G S *et al*. *Materials Science and Engineering A*[J], 2023, 886: 145669
50 Liu K W, Fang F, Tu Y Y *et al*. *Materials Science and Engineering A*[J], 2023, 870: 144853
51 Wang Hongwei, He Zhufeng, Jia Nan. *Acta Metallurgica Sinica*[J]. 2021, 57(5): 632 (in Chinese)
52 Luo Z Y, Li J H, Feng T F *et al*. *Materials Science and Engineering A*[J], 2023, 885: 145623
53 Zhao Y N, Chen Z W, Yan K *et al*. *Materials Science and Engineering A*[J], 2023, 866: 144690
54 Cao Yuhan, Wang Lilin, Wu Qingfeng *et al*. *Acta Metallurgica Sinica*[J], 2020, 56(3): 333 (in Chinese)
55 Cheng J C, Li N, Xia P *et al*. *Materials Letters*[J], 2024, 358: 135834
56 Luo Z Y, Feng T F, Li C *et al*. *Materials Science and Engineering A*[J], 2024, 899: 146433
57 Jiang F L, Zhao C C, Liang D S *et al*. *Materials Science and Engineering A*[J], 2020, 771: 138625
58 Wang P, Ren P, Wu X *et al*. *Materials Science and Engineering A*[J], 2022, 858: 144192
59 Shen J J, Choi Y T, Yang J *et al*. *Materials Science and Engineering A*[J], 2024, 896: 146272
60 Peng S Y, Feng S, Jiang Z F *et al*. *Materials Research Letters*[J], 2024, 12(5): 363
61 Lin P T, Liu H C, Hsieh P Y *et al*. *Materials & Design*[J], 2021, 197: 109238
62 He L, Wu S W, Dong A P *et al*. *Journal of Materials Science & Technology*[J], 2022, 117: 133
63 Kim Y K, Baek M S, Yang S *et al*. *Additive Manufacturing*[J], 2021, 38: 101832
64 Kim Y K, Kim M C, Lee K A. *Journal of Materials Science & Technology*[J], 2022, 97: 10
65 Han D, Yang B J, Xu W L *et al*. *Journal of Materials Science & Technology*[J], 2024, 193: 1
66 Jin X, Liang Y X, Zhang L *et al*. *Materials Science and Engineering A*[J], 2019, 745: 137
67 Gao X F, Chen Y, Ren H *et al*. *Transactions of Nonferrous Metals Society of China*[J], 2020, 34(3): 890
68 Ye X C, Lei, H F, Liu, X W *et al*. *Materials Letters*[J], 2023, 343: 134395
69 Xiong T, Zheng S J, Pang J Y *et al*. *Scripta Materialia*[J], 2020, 186: 336
70 Liu L Y, Zhang Y, Zhang Z W *et al*. *Materials Science and*

Engineering A[J], 2023, 882: 145413
71 Lu T W, He T B, Zhao P P *et al*. *Journal of Materials Processing Technology*[J], 2021, 289: 116945
72 Liu D, Hou J X, Jin X *et al*. *Intermetallics*[J], 2023, 163: 108064
73 Zhou S C, Dai C D, Hou H X *et al*. *Scripta Materialia*[J], 2023, 226: 115234
74 Xiao B, Chen R, Zhang J Y *et al*. *Additive Manufacturing*[J], 2023, 77: 103795
75 Sun W T, Fu Y, Ma H *et al*. *Materials Science and Engineering A*[J], 2023, 887: 145757
76 Zhang C, Zhu C Y, Cao P H *et al*. *Acta Materialia*[J], 2020, 199: 602
77 Wang J S, Ke Y J, Chen Y F *et al*. *Journal of Materials Research & Technology*[J], 2023, 27: 8119
78 Ma Y X, Zhang Y, Sun L X *et al*. *Journal of Materials Science & Technology*[J], 2024, 192: 215
79 Li Z J, Fu P X, Chen L *et al*. *Materials Science and Engineering A*[J], 2024, 880: 145326
80 Zhou Y K, Zeng S, Zhang H W *et al*. *Journal of Materials Science & Technology*[J], 2024, 187: 101
81 Tripathy B, Ojha P K, Bhattacharjee P P. *Journal of Alloys and Compounds*[J], 2023, 948: 169783
82 Reddy S R, Sunkari U, Lozinko A *et al*. *Intermetallics*[J], 2019, 114: 106601
83 Liu L Y, Zhang Y, Zhang Z W *et al*. *International Journal of Plasticity*[J], 2024, 172: 103853
84 Zhang C, Zhu C Y, Harrington T *et al*. *Scripta Materialia*[J], 2018, 154: 78
85 Zhang C, Zhu C Y, Vecchio K. *Materials Science and Engineering A*[J], 2019, 743: 361
86 Wang J P, Zhang Z, Dai H L *et al*. *Corrosion Science*[J], 2022, 209: 110761
87 Zhang Z, Zhai X Y, Chen G *et al*. *Scripta Materialia*[J], 2022, 213: 114591
88 Zhang Z, Zhai X Y, Anggraini L *et al*. *International Journal of Fatigue*[J], 2024, 182: 108185
89 Shi L H, Zhang Z, Chen X. *International Journal of Fatigue*[J], 2023, 172: 107656
90 An Z B, Mao S C, Liu Y N *et al*. *Journal of Materials Science & Technology*[J], 2021, 92: 195
91 Luo J S, Sun W T, Duan R X *et al*. *Journal of Materials Science & Technology*[J], 2022, 110: 43
92 Chen J X, Li T, Chen Y *et al*. *Acta Materialia*[J], 2023, 243: 118515
93 Gao X Y, Liu J, Fu W J *et al*. *Materials & Design*[J], 2023, 233: 112250
94 Zou Y, Li S L, Li Y. *Surface & Coatings Technology*[J], 2022, 441: 128558
95 Miao X L, Liu G, Xu C C *et al*. *Intermetallics*[J], 2024, 164: 108107
96 Dasari S, Jagetia A, Chang Y J *et al*. *Journal of Alloys and Compounds*[J], 2020, 830: 154707
97 Zhao Y N, Chen Z W, Yan K *et al*. *Materials Science and Engineering A*[J], 2022, 838: 142759
98 Zhang C, MacDonald B E, Guo F W *et al*. *Scripta Materialia*[J], 2020, 188: 16
99 Sun B, Wang Q Q, Chen Y X *et al*. *Journal of Alloys and Compounds*[J], 2023, 953: 170066
100 Son S J, Lee J W, Asghari-Rad P *et al*. *Materials Research Letters*[J], 2023, 11(11): 915
101 Yang Z S, Liu X, Zhao J J *et al*. *International Journal of Plasticity*[J], 2024, 176: 103963
102 He M Y, Shen Y, Jia N *et al*. *Journal of Alloys and Compounds*[J], 2023, 939: 168831
103 Qin S, Yang M X, Jiang P *et al*. *Materials Characterization*[J], 2022, 186: 111779
104 Nartu M, Chesetti A, Sharma A *et al*. *Materials Science and Engineering A*[J], 2022, 849: 143505
105 Zhu Z G, An X H, Lu W J *et al*. *Materials Research Letters*[J], 2019, 7(11): 453
106 Guo Y N, Su H J, Zhou H T *et al*. *Journal of Materials Science & Technology*[J], 2022, 111: 298
107 Wang P F, Chen J, Sun B T *et al*. *Materials Science and Engineering A*[J], 2022, 840: 142880
108 Gu G H, Kim R E, Kim E S *et al*. *Journal of Materials Research and Technology*[J], 2022, 21: 2880
109 Gu J, Ni S, Liu Y *et al*. *Materials Science and Engineering A*[J], 2019, 755: 289
110 Li Y, Wang Q M, Xu C *et al*. *Materials Science and Engineering A*[J], 2024, 906: 146708
111 Song M, Zhou R, Gu J *et al*. *Applied Materials Today*[J], 2020, 18: 100498
112 Tung S Y, Hsu T E, Zhu Y T *et al*. *Acta Materialia*[J], 2024, 273: 119957
113 An Z B, Mao S C, Jiang C. *Scripta Materialia*[J], 2024, 239: 115809
114 Yang G H, Kim J K. *Acta Materialia*[J], 2022, 233: 117974
115 Xiao Y K, Peng X H, Fu T. *Advanced Powder Technology*[J], 2022, 33: 103520
116 Chen H Y, Gou J M, Jia W T *et al*. *Acta Materialia*[J], 2024, 246: 118702
117 Guo Y N, Su H J, Yang P X *et al*. *Additive Manufacturing*[J], 2022, 60: 103257
118 Fu Z H, Zhang Y, Li Z M *et al*. *Journal of Materials Research and Technology*[J], 2023, 24: 3300
119 You Z Y, Tang Z Y, Chu F *et al*. *Intermetallics*[J], 2023, 156: 107854
120 Lv J L, Zhou Z P, Tong L *et al*. *Journal of Alloys and Compounds*[J], 2023, 934: 167791
121 Sathiyamoorthi P, Asghari-Rad P, Park J M *et al*. *Materials Science and Engineering A*[J], 2020, 766: 138372
122 Zhang L, Du X H, Zhang L. *Vacuum*[J], 2021, 188: 110169
123 Ding Z Y, Xie J T, Wang T *et al*. *Materials Science and Engineering A*[J], 2024, 891: 145942
124 Peng H L, Huang S M, Hu L *et al*. *Intermetallics*[J], 2024, 166: 108182

125 Slone C E, Miao J, George E P *et al*. *Acta Materialia*[J], 2019, 165: 496
126 Li Z J, Chen L, Su H H *et al*. *Materials Science and Engineering A*[J], 2022, 852: 143655
127 Wang Y F, Ma X L, Guo F J *et al*. *Materials & Design*[J], 2023, 225: 111593
128 Sun S J, Tian Y Z, Lin H R *et al*. *Materials Science and Engineering A*[J], 2019, 740–741: 336
129 Liu S L, Luo K G, Gu H *et al*. *Scripta Materialia*[J], 2023, 222: 115004
130 Haftlang F, Asghari-Rad P, Moon J *et al*. *Scripta Materialia*[J], 2022, 202: 114013
131 Moon J, Park J M, Wung J *et al*. *Acta Materialia*[J], 2020, 193: 71
132 Lee J, Bae J W, Asghari-Rad P *et al*. *Scripta Materialia*[J], 2022, 211: 114511
133 Wei R, Gao Q Y, Zhang X H *et al*. *Materials Science and Engineering A*[J], 2024, 867: 144710
134 Jia Z Y, Zhang S Z, Huo J T *et al*. *Materials Science and Engineering A*[J], 2022, 834: 142617
135 Han Z H, Li J Z, Tian Y B *et al*. *Intermetallics*[J], 2023, 159: 107933
136 Chang R B, Fang W, Yu H Y *et al*. *Scripta Materialia*[J], 2023, 172: 144
137 Zhang D D, Zhang J Y, Kuang J *et al*. *Acta Materialia*[J], 2022, 233: 117981
138 Jiang Z, Wei R, Wang W Z *et al*. *Journal of Materials Science & Technology*[J], 2022, 100: 20
139 Lu W J, Luo X, Ning D *et al*. *Journal of Materials Science & Technology*[J], 2022, 112: 195
140 Yang M X, Yan D S, Yuan F P *et al*. *Proceedings of the National Academy of Sciences*[J], 2018, 115(28): 7224
141 Wen R, You C P, Zeng L F *et al*. *Journal of Materials Science*[J], 2020, 55: 12544
142 Li A X, Liu X S, Li R. *Journal of Materials Science & Technology*[J], 2024, 181: 176
143 Lu W J, Yan K, Luo X *et al*. *Journal of Materials Science & Technology*[J], 2022, 98: 197
144 Chou T, Li W, Chang H *et al*. *Scripta Materialia*[J], 2023, 299: 115377
145 Wang J Y, Zou J P, Yang H L *et al*. *Journal of Materials Science & Technology*[J], 2022, 127: 61
146 Xu D F, Zhang H T, Wang M L *et al*. *Materials Science and Engineering A*[J], 2022, 860: 114293
147 Han Z H, Tian Y B, Yang J *et al*. *Intermetallics*[J], 2024, 164: 108129
148 Yao N, Lu T W, Feng K *et al*. *Acta Materialia*[J], 2022, 236: 118142
149 Du X H, Li W P, Chang H T. *Nature Communications*[J], 2020, 11: 2390
150 Zhang Z H, Jiang P, Yuan F P *et al*. *Materials Science and Engineering A*[J], 2022, 832: 142440
151 Gao Q Y, Zhang X H, Feng S L *et al*. *Journal of Materials Science & Technology*[J], 2024, 183: 175
152 Han B L, Zhang C C, Feng K *et al*. *Materials Science and Engineering A*[J], 2021, 820: 141545
153 Haftlang F, Zargaran A, Moon J *et al*. *Journal of Alloys and Compounds*[J], 2023, 968: 171870
154 Haftlang F, Kim E S, Kwon J *et al*. *Additive Manufacturing*[J], 2023, 63: 103421
155 Wang J Y, Zou J P, Yang H L *et al*. *Journal of Materials Science & Technology*[J], 2023, 135: 241
156 Yang Y, Chen J Y, Ma T X *et al*. *Rare Metal Materials and Engineering*[J], 2022, 51(9): 3182

单级和多级异质结构调控中/高熵合金的微观组织及性能优化研究进展

王　炳[1,2]，李春燕[1,2,3]，王新华[2]，李晓诚[1,2]，寇生中[1,2,3]
(1. 兰州理工大学 省部共建有色金属先进加工与再利用国家重点实验室，甘肃 兰州 730050)
(2. 兰州理工大学 材料科学与工程学院，甘肃 兰州 730050)
(3. 兰州理工大学 温州泵阀工程研究院，浙江 温州 325105)

摘　要：开发高性能结构/功能材料对于大多数工业领域具有重要的意义。中/高熵合金因其特定的微观结构表现出优异的综合性能，是极具潜力的结构材料。更重要的是，通过调控合金的微观组织并优化其性能已经成为拓展合金工业应用的重要措施。已有的研究表明，构建多种异质结构有利于显著提升中/高熵合金的综合性能。本文详细讨论了具有单级和多级异质性的多异质结构。此外，还系统地综述了中/高熵合金中成分不均匀性、双峰结构、双相结构、片状/层状结构、谐波结构（核壳）、多尺度沉淀物及特定微观结构耦合异质结构的制备方法。深入讨论了不同异质结构诱发的变形机制，以探索异质结构与中/高熵合金性能优化之间的关系。全面阐释了异质结构和先进的微观结构优化中/高熵合金性能的贡献，以进一步改善合金的性能。最后，讨论了高性能中/高熵合金未来在工业应用中的挑战，并尝试为优化异质结构提高中/高熵合金综合性能提供可行的方法。

关键词：异质结构；中/高熵合金；异质变形诱导效应；微观组织调控；性能优化

作者简介：王　炳，女，1993年生，博士生，兰州理工大学省部共建有色金属先进加工与再利用国家重点实验室，E-mail：ztswbing@163.com